IN-07
9532

NASA Technical Memorandum 4777

Design and Laboratory Validation of a Capacitive Sensor for Measuring the Recession of a Thin-Layered Ablator

Gregory K. Noffz and Michael P. Bowman

November 1996

NASA Technical Memorandum 4777

Design and Laboratory Validation of a Capacitive Sensor for Measuring the Recession of a Thin-Layered Ablator

Gregory K. Noffz and Michael P. Bowman
Dryden Flight Research Center
Edwards, California

National Aeronautics and
Space Administration

Office of Management

Scientific and Technical
Information Program

1996

CONTENTS

TABLE

FIGURES

ABSTRACT

Flight vehicles are typically instrumented with subsurface thermocouples to estimate heat transfer at the surface using inverse analysis procedures. If the vehicle has an ablating heat shield, however, temperature time histories from subsurface thermocouples no longer provide enough information to estimate heat flux at the surface. In this situation, the geometry changes and thermal energy leaves the surface in the form of ablation products. The ablation rate is required to estimate heat transfer to the surface. A new concept for a capacitive sensor has been developed to measure ablator depth using the ablator's dielectric effect on a capacitor's fringe region. Relying on the capacitor's fringe region enables the gage to be flush mounted in the vehicle's permanent structure and not intrude into the ablative heat shield applied over the gage. This sensor's design allows nonintrusive measurement of the thickness of dielectric materials, in particular, the recession rates of low-temperature ablators applied in thin (0.020 to 0.060 in. (0.05 to 0.15 mm)) layers. Twenty capacitive gages with 13 different sensing element geometries were designed, fabricated, and tested. A two-dimensional finite-element analysis was performed on several candidate geometries. Calibration procedures using ablator-simulating shims are described. A one-to-one correspondence between system output and dielectric material thickness was observed out to a thickness of 0.055 in. (1.4 mm) for a material with a permittivity about three times that of air or vacuum. A novel method of monitoring the change in sensor capacitance was developed. This technical memorandum suggests further improvements in gage design and fabrication techniques.

NOMENCLATURE

Acronyms

BNC	bayonet navy connector
BRAG	backscatter radiation ablation gage
PC	printed circuit
RAT	radiation transducer (sensor)
RCB	reflection coefficient bridge
RF	radio frequency
RLC	resistive, inductive, and capacitive termination to a waveguide
RTV	room-temperature vulcanized silicon
RV	reentry vehicle
SCAT	shape change ablation transducer
TC	thermocouple
TPS	thermal protection system

Symbols

a	length dimension, m or cm
b	length dimension, m or cm
C	capacitance, pF
c_p	specific heat, J/kg-K
E	stored electric energy per unit length, J/m or J/cm
f_o	resonant frequency, MHz
k	thermal conductivity, W/m · K
L	unit length, m or cm, or inductance, H
$q_{conduction}$	conduction heat flux, W/m^2
$q_{convection}$	convective heat flux, W/m^2
$q_{radiation}$	radiation heat flux, W/m^2
R_{max}	maximum radius, m
V	electric potential, V
α	angle between plates, rad
ε	permittivity, (C^2/N · m^2)
ρ	charge density, C/m^3
ρ_m	mass density, kg/m^3

INTRODUCTION

Aerospace vehicles subjected to significant aerodynamic heating often rely on ablating thermal protection systems (TPSs) to keep the internal structure and equipment below critical operating temperatures. An ablating TPS undergoes chemical decomposition or phase change (or both) below the internal structure's critical temperature. Incident thermal energy is then channeled into melting, subliming, or decomposing the ablator. Ablator recession rate is directly proportional to the heat flux at the surface. Unless a char layer forms, the surface remains at ablation temperature as ablation products are blown into the airstream. As long as some virgin ablator remains, the substructure does not exceed ablation temperature. Figure 1 depicts a schematic of an ablating surface.

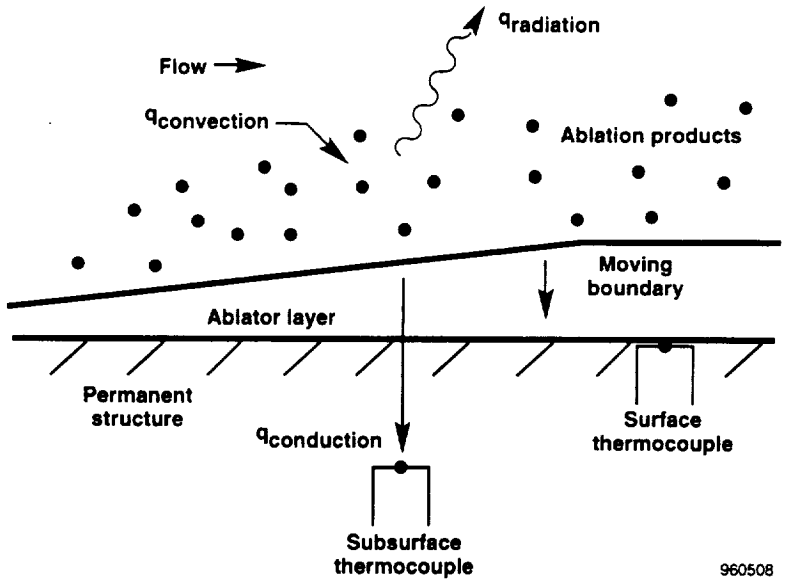

Figure 1. Ablation situation.

Measuring the heat flux to an ablating vehicle presents a difficult challenge. Several operational problems arise with embedding heat-flux gages or thermocouples in an ablating TPS. First, as the ablator recedes, the gage's sides are exposed to the airstream. The thermal input to the gage's side invalidates calibrations where the temperature gradient is assumed to be normal to the gage's sensing face. Second, any protruding object affects the recession rate of the surrounding ablator. Third, ablation products may contaminate the sensor's face. Finally, after ablation begins, temperatures often attain a steady state where recession rate is proportional to heat flux. A measure of ablator thickness is now required to estimate surface heat flux.

The measurement method must not affect the recession rate or severely alter the conduction path through the ablator; to ensure this, the sensor is located in the permanent structure below the ablating layer. The sensor should be insensitive to temperature and, over the expected temperature range, be capable of calibration.

Background

Past efforts to measure recession of TPSs have concentrated on nosetips of ballistic reentry vehicles (RVs). RVs typically experience very high heating rates and are constructed with relatively thick, high-temperature ablators when compared with vehicles subjected only to ascent heating. Sensors developed for RVs can be grouped into two categories, intrusive and nonintrusive. The intrusive concepts involve installing hardware in the ablator or seeding the ablator with radioactive material. Nonintrusive methods rely on sensors and hardware in the substructure below the ablator.

Legendre (ref. 1) surveys instrumentation techniques tested or proposed through 1975. Intrusive recession measurement techniques include the breakwire ablation gage, radiation transducer (RAT) sensor, and light pipe. The breakwire ablation gage consists of several thin wires implanted at various known levels in an ablator. As the material progressively erodes, each successive wire is broken and results in an open circuit. Figure 2 illustrates this concept. In some cases (ref. 2), each breakwire doubles as a thermocouple (TC) and each is situated so that no breakwire TC is directly above another. This arrangement allows an unobstructed conduction path through the ablator to each breakwire TC, including those at lower levels. Although the breakwire method provides temperature time histories until the last TC is exposed and destroyed, this method only provides recession data at a few distinct points.

As another intrusive method, the RAT sensor relies on small radioactive sources placed at known depths within the TPS. As the ablator recedes, radiation sources are removed and the reduction in radiation is measured by a Geiger counter (ref. 1). A variation of this method is the shape change ablation transducer (SCAT). Implemented behind a graphite nosetip uniformly seeded with

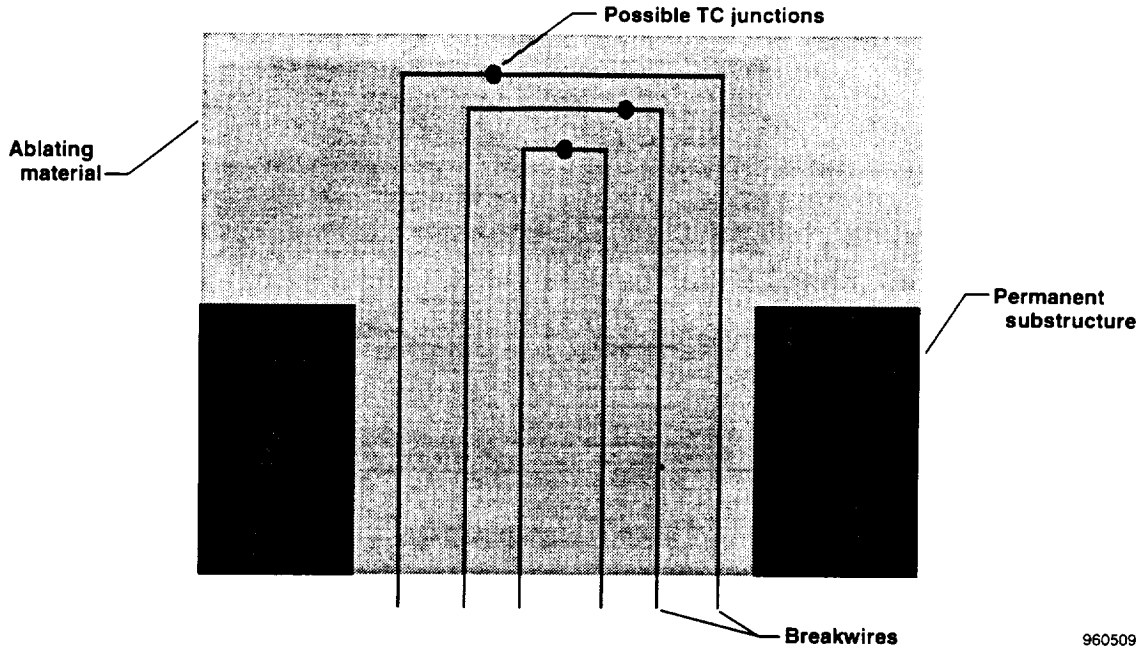

Figure 2. Breakwire ablation gage.

radioactive material, the SCAT detects recession in areas away from the nosetip using moving radiation detectors. The RAT sensor provides distinct data points corresponding to the number of implant sources, whereas the SCAT provides continuous data. Only the RAT sensor has met with operational success.

The light pipe sensor consists of quartz fibers implanted in an ablator and terminated at known depths (fig. 3). When the TPS recedes to where a fiber terminates, light transmits down to a photodiode. Arrays of lightpipes have been used in nosetips to ascertain shape change up to three nose radii aft of the tip. This method provides recession data at distinct points only and does not provide temperature data, as the breakwire method does.

An example of a nonintrusive sensor is the backscatter radiation ablation gage (BRAG). The BRAG consists of a gamma ray source and detector unit. The radiation amount that is reflected from the ablator is directly proportional to its thickness. According to Legendre (ref. 1), this sensor provides a useful method of measuring recession on graphite nosetips without disturbing the material.

Armini and Bunker (ref. 3) developed a sensor concept with gamma ray detectors, as in the BRAG concept; however, this sensor has radioactive "line" sources implanted in the nosetip. A completed graphite nosetip is subjected to high-energy proton beams from a linear accelerator. The portion of graphite that the beam passes through becomes radioactive, that is, the line source. The advantage of this sensor is that many line sources can be induced in a single nosecap, thus indicating recession away from the stagnation point.

McGunigle and Jennings (ref. 4) described an ultrasonic nosetip recession sensor. This instrument emits sound waves and then measures the time required for the echo to return from the ablator surface. This sensor was successfully tested on the ground and in flight. Ground tests involved placing an instrumented nosetip in an arc-jet tunnel or rocket exhaust facility and comparing sensor output with motion-picture footage of the test. The sensor, essentially a microphone, detected not only the echo from the ablator surface but also any aerodynamic noise from the rocket exhaust, thus making ground tests more difficult. As the ablator (in this case, graphite, carbon composites, or metals) began to recede, a change in the speed of sound within the ablator due to elevated temperatures distorted the recession measurements.

The sensors discussed above share some or all of the following traits that make them unsuitable for

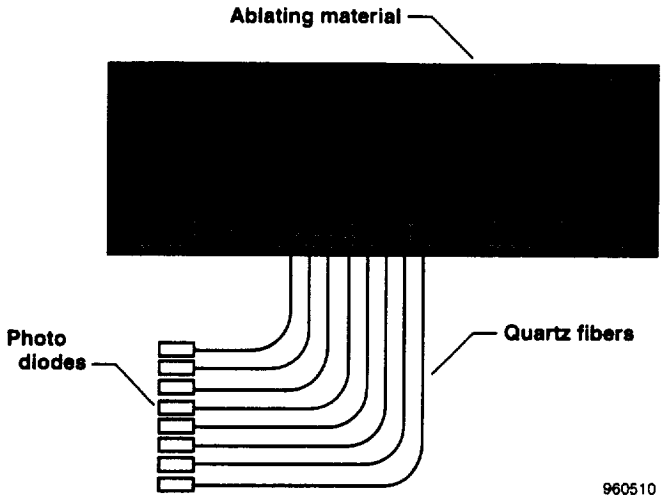

Figure 3. Light pipe gage.

measuring recession of the relatively thin thermal protection systems found on booster vehicles:

- Resolution is of the order of the ablator thickness (0.015 to 0.060 in. or 0.381 to 1.524 mm).
- Hardware tends to be large or have high power requirements (or both).
- Signal-to-noise ratios are low.
- The handling of radioactive materials is required.

Of these sensor concepts, the ultrasonic ablation measurement system comes closest to being usable for thin TPSs: it is nonintrusive and does not involve radioactive materials. Instrumentation concepts better suited for use with thin TPSs, however, were found in connection with work on measuring thin liquid films.

Thin Film Work

Brown et al. (ref. 5) determined liquid film thickness by measuring the capacitance between two small wire probes protruding into the liquid. The liquid acted as a dielectric between two plates of a capacitor with the plates being two small wire probes (fig. 4). If the liquid has a different dielectric constant than air, a change in liquid level results in a change in the probe's capacitance.

Benn (ref. 6) was interested in measuring film thicknesses of electrically conducting liquids. This approach involved installing two metal probes flush with the wall and measuring the electrical resistance between them. As the film got thinner, the resistance increased. This method was nonintrusive to the film layer and was unhindered by surface tension considerations, as the Brown probe was. Eventually, Benn wanted to measure film thicknesses of a nonconducting liquid, Freon 12. The same probe was used, but it measured the capacitance between the two probe elements. This technique was distinctive from other methods of measuring film thickness in that the liquid was not directly between the plates of the capacitive probe. The liquid affected only the capacitor's fringe field lines. This layout lowered the sensitivity but eliminated problems such as the liquid clinging to the probe by surface tension. Gage output was affected by changes in temperature and lead wire position. Figure 5 shows the probe geometry, with one lead being a metal tube and the second lead being a wire suspended within. The entire length of the probe assembly contributed to its total capacitance. The probe capacitance increased, but the percentage change due to changes in film thickness decreased.

The capacitance changes were measured by incorporating the probe into a frequency modulation circuit. A fixed frequency was the input to the circuit, and the output frequency depended on probe capacitance. The output frequency was channeled through various filters, rectifiers, and linearizers until the system produced a DC voltage that varied linearly with film thickness.

The research described in this memorandum builds on the thin film work of Benn and attempts to adopt this concept to measuring ablator layer thicknesses, in particular, those designed to protect launch vehicles like

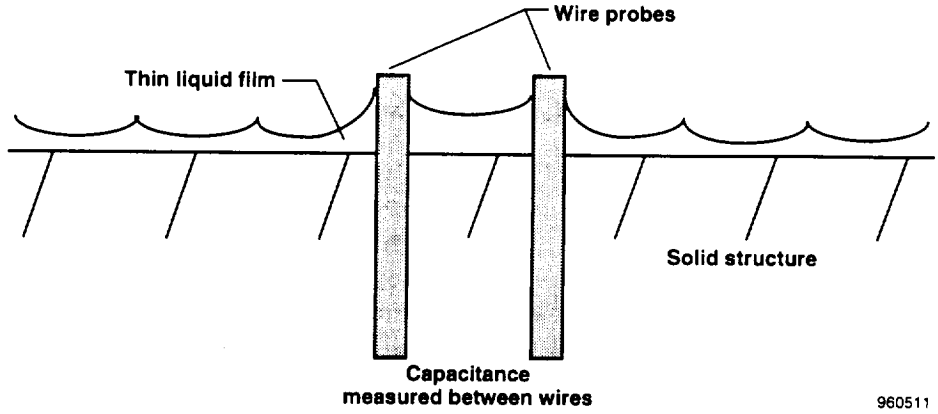

Figure 4. Brown's thin film probe.

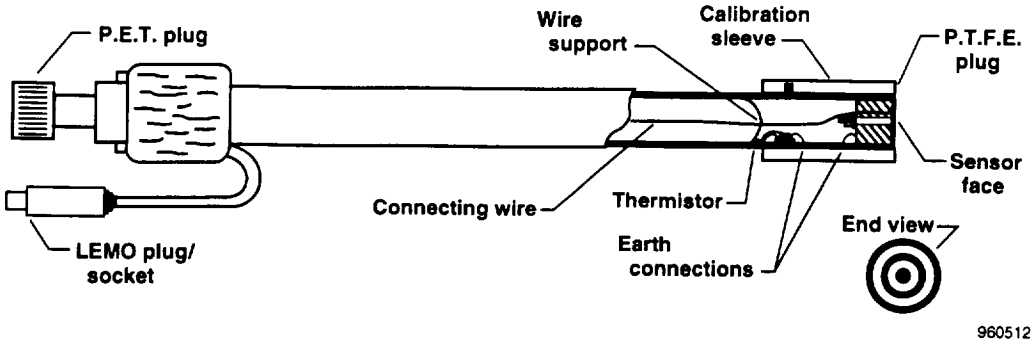

Figure 5. Benn's test probe (from ref. 6).

the Pegasus® from ascent heating (ref. 7). Before this sensor concept can be used on flight vehicles, several modifications must be made.

- First, the gage sensitivity must be increased to give a high-level output. This increase makes the task of signal conditioning and calibration easier.
- Second, the probe's total capacitance must be contained as much as possible in the sensing part of the probe, reducing the effect of lead-wire position and temperature.
- Third, the effect of gage temperature on the measurement must be minimized with proper fabrication techniques.
- Fourth, the probe's size itself must be much smaller for flight applications.

This memorandum documents the evolution of the sensor concept. Candidate designs were evaluated and compared based on sensitivity, usable range of dielectric thickness, and ease of fabrication. To determine general trends, various gage geometries were modeled and evaluated using a commercially available finite-element code. Operational issues such as fabrication, system shielding and packaging, and calibration are discussed.

Use of trade names or names of manufacturers in this document does not constitute an official endorsement of such products or manufacturers, either expressed or implied, by the National Aeronautics and Space Administration.

SYSTEM OVERVIEW

As mentioned earlier, Benn used the capacitive probe as part of a frequency modulation circuit. The present work used a different concept that takes advantage of off-the-shelf hardware used for antenna tuning. The capacitive sensor is placed in series with an inductor and a resistor forming an resistive, inductive, and capacitive

® Pegasus is a trademark of Orbital Sciences Corp., Fairfax, Virginia.

(RLC) termination to a waveguide (i.e., a coaxial cable). The arrangement shown in figure 6 is very similar to a transmitter-antenna configuration. The RLC termination has a resonant frequency approximated by

$$f_o \approx \frac{1}{2\pi\sqrt{LC}} \qquad (1)$$

When electromagnetic energy at the resonant frequency is sent down the waveguide, all the energy dissipates in the resistor. If, however, the resonant frequency of the termination changes (say, because of a change in capacitance), a fraction of the energy is reflected back toward the source. As the capacitance continues to change, the energy reflected increases. Antennas that work like this are said to be out of tune. In this situation, one could use a commercially available reflection coefficient bridge (RCB) between the radio frequency (RF) source and the waveguide termination. The RCB generates a DC voltage proportional to the energy reflected. Then the antenna can be adjusted until the bridge output voltage is a minimum and the energy transmitted is a maximum.

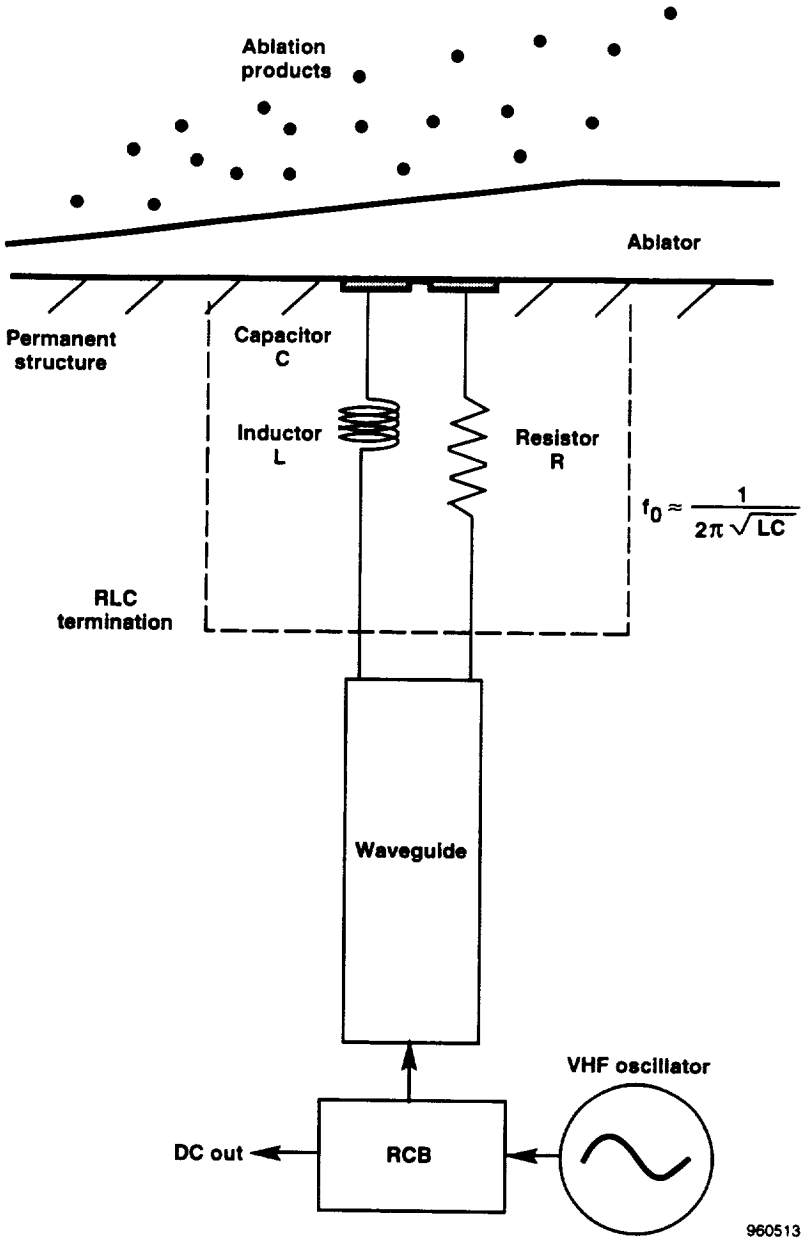

Figure 6. System setup.

This concept is the basis for the probe's system circuitry (fig. 6). The probe, along with the inductor and resistor that form the RLC termination, is connected via coaxial cable to a signal generator. A reflection coefficient bridge is placed between the signal generator and the probe, and output to a voltmeter (for static measurements and calibrations) or data recorder (for transient measurements). Figure 7 is a photograph of the bench test setup. The sensor mounts in the aluminum plate at the front of the table. The signal generator is in the background, and the small aluminum box next to the multimeter is the RCB. The basic procedure involves varying the frequency of the signal generator until the bridge output is a minimum (ideally near zero) while the face of the probe is exposed only to air. Delrin® shims of similar dielectric constant to the ablator and known thicknesses are then placed on the probe face. Capacitance (and RCB output) increases with shim thickness, and a calibration curve is obtained.

CANDIDATE DESIGNS, FABRICATION, AND PACKAGING

To increase sensitivity of a flush capacitive sensor to changes in dielectric thickness, the volume directly between the conductors must be minimized by making them as thin as possible. This design maximizes the fraction of total gage capacitance that the fringe field lines account for.

The first candidate design (fig. 8) consists of two concentric brass rings 0.1 in. (2.54 mm) thick with the outer ring 0.5 in. (12.7 mm) in diameter. A Delrin chassis holds the rings concentric. This design has a room-temperature capacitance of 4.7 pF. The design is a direct descendant of the Benn probe and served as a gage prototype for setting up the system circuitry. Using this gage proved that small percentage changes in gage capacitance resulting from simply passing one's hand over the gage surface could be monitored. Because it was quickly realized that a different fabrication method would further increase sensitivity while simultaneously providing a convenient method to mount the other required electrical components, no real testing of this design was undertaken.

To minimize the thickness of the conductors, probes were made from raw circuit board material using standard techniques for printed circuit (PC) board fabrication. Figure 9 shows some candidate geometries. All geometries have a surface area of 0.25 in^2 (about 161 mm^2). The concentric circle geometries connect every other circle to a trace on the backside of the

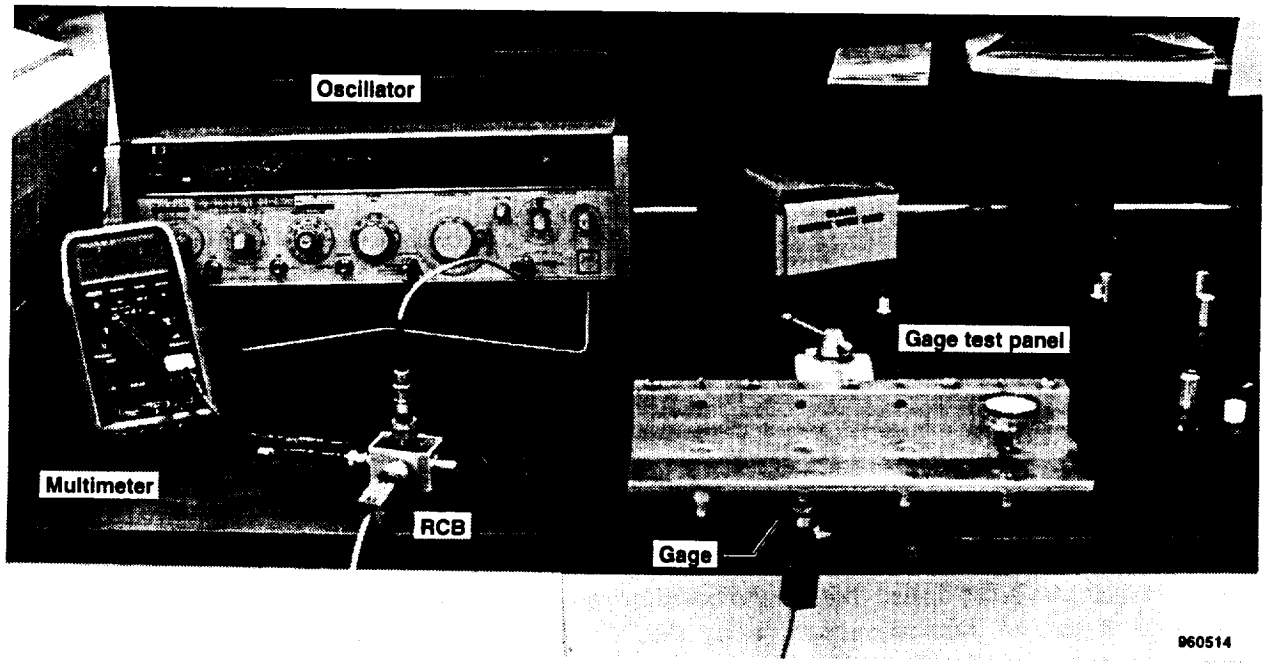

Figure 7. Static measurement test setup with oscillator, reflection coefficient bridge, multimeter, and gage.

® Delrin is a trademark of Dupont, Wilmington, Delaware.

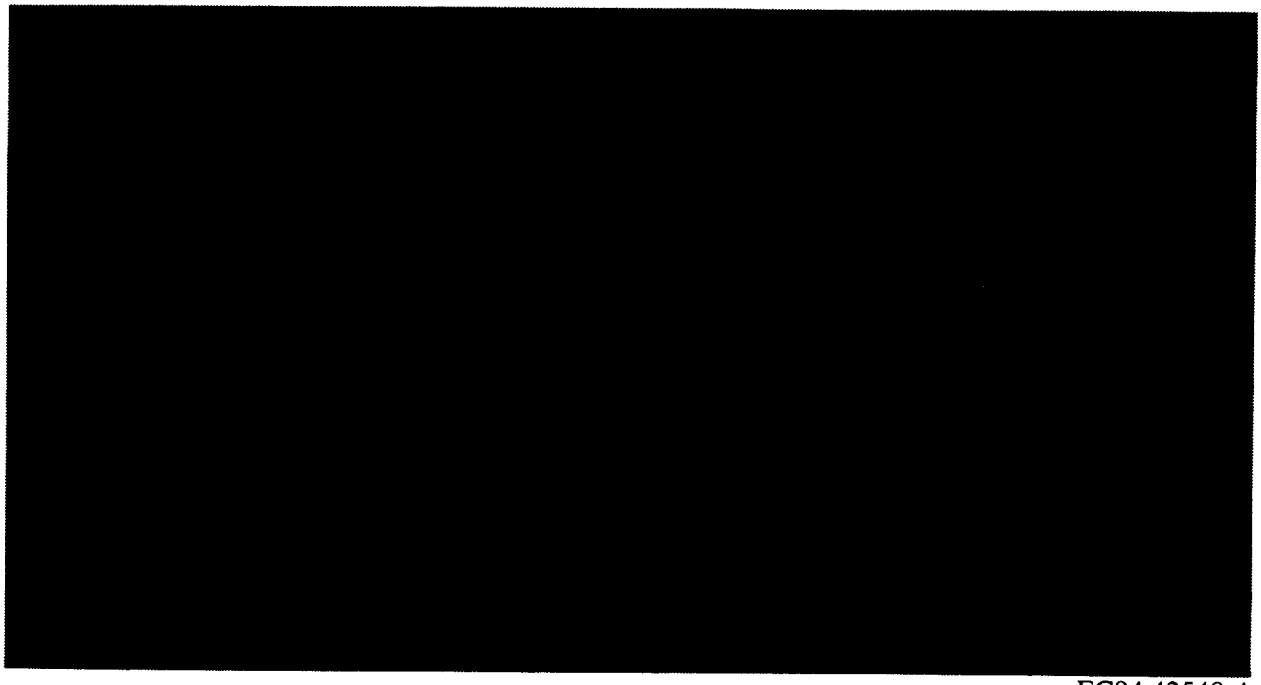

EC94 42548-4

Figure 8. Brass ring gage.

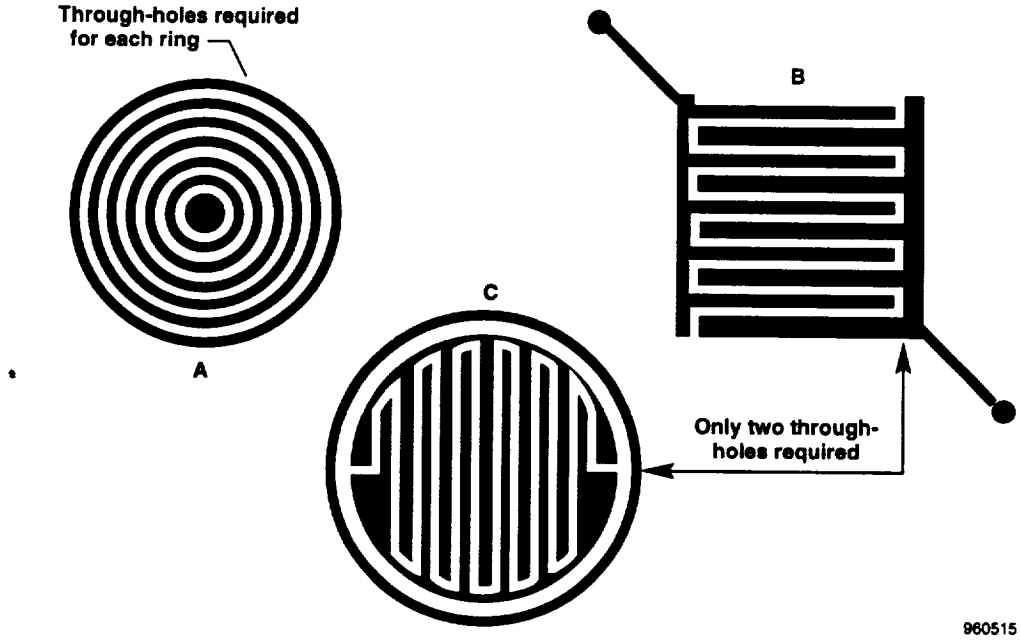

Figure 9. Candidate geometries.

PC board. This design requires two-sided circuit boards with many connection holes drilled through the board. This presents a tedious fabrication task when the conductors become narrow. The square geometries and the nonconcentric round geometries require only two through-holes because the capacitor is composed of only two plates. Consequently, only the round, nonconcentric geometries, item C in figure 9, were pursued further.

Some preliminary tests were performed on circuit-board gages with the associated electronic components attached to the board near the gage itself (fig. 10). A more desirable arrangement, however, combines the

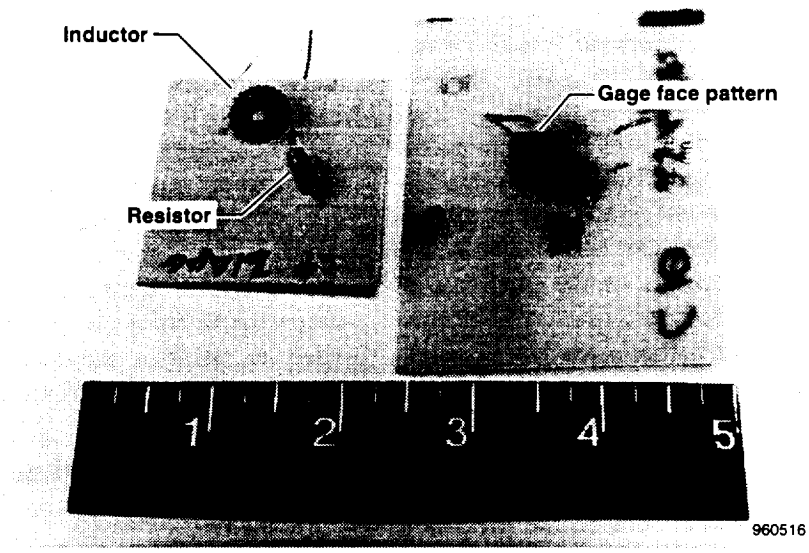

Figure 10. First-generation gages.

RLC portion of the system into a single, shielded unit that can be handled without fear of changing gage output due to changes in lead-wire location or inductor windings. Figure 11 shows such a unit. The prototype gages consist of a brass casing (later prototypes used aluminum) surrounding a Delrin chassis that holds the inductor and resistor. The gage face mounts on the surface of the Delrin, flush with the end of the casing. A male bayonet navy connector (BNC) installs in the rear of the casing opposite the sensing face. The brass casing connects to the shield side of the incoming coaxial cable, thus shielding all components except the sensing element itself. The entire assembly is held together and potted with standard room-temperature vulcanized (RTV) silicon. Although this design is robust and easy to handle and mount in test fixtures, the use of RTV in lieu of mechanical fasteners makes it unsuitable for elevated temperatures.

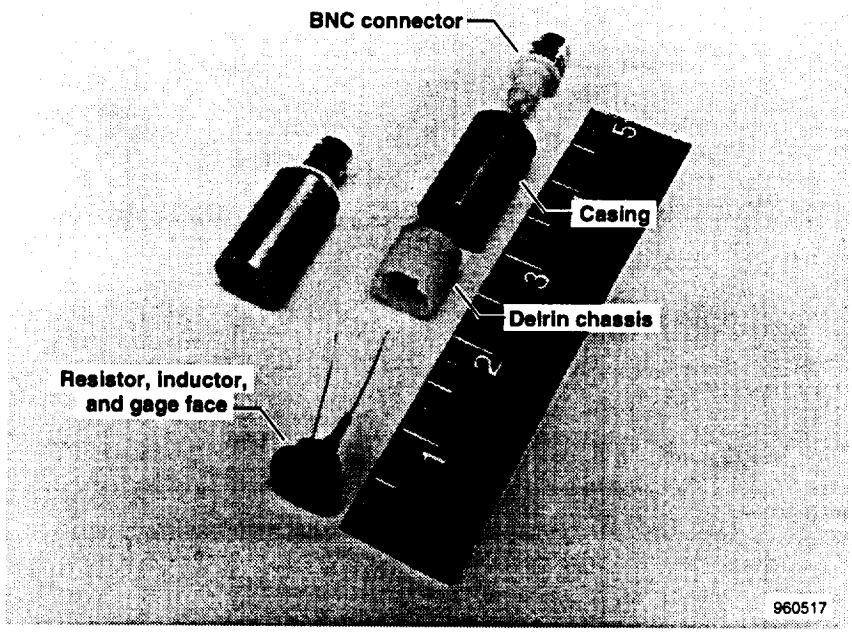

Figure 11. Second-generation gage before and after final assembly.

The pattern of the capacitor itself (item C in fig. 9), while circular, does not require the extensive through-hole connections like the concentric circle pattern (item A in fig. 9) previously discussed. Initially, 12 plug-type gages were fabricated using nine of these nonconcentric round geometries with two of the geometries duplicated. After testing, 8 more gages were fabricated, for a total of 20. The last eight gages used faces etched by a company that fabricates circuit boards. Using these allowed the conductors on the gage face to connect to the backside of the board via plated through-holes, eliminating the solder bumps of the first 12 gages. The first 12 sensor casings were fabricated from brass in anticipation of soldering the shield side of the coaxial cable to the casing. During the fabrication process, a method of press-fitting a small terminal post to the inside of the casing (fig. 12) eliminated the need for a solder joint to the brass. All 20 gages use this terminal post arrangement, but the design allowed the last eight casings to be fabricated from aluminum. To further miniaturize the gage, the aluminum casings were initially made 0.1 in. (2.54 mm) shorter for an overall length of 1.13 in. (28.32 mm).

THEORY AND MODELING

Early in the prototyping process it became apparent that the sensor face configurations would consist of alternating capacitor plates on a flat substrate, as shown in figure 13. Preliminary tests also showed that several factors, including calibration procedures, slight variations in system setup, and manufacturing tolerances, could affect results. Because one purpose of this study was to determine the optimal sensor geometry (i.e., conductor width and gap configuration), we compared sensor geometries using analytical and computational methods that eliminate experimental errors. In this section, analytical approximations are explored and two-dimensional, finite-element analyses of some gage geometries using a commercially available code that calculates electrostatic fields (ref. 8) are described.

Analytical Models

The literature about calculating parasitic capacitances of integrated circuits is one source for analytical approximations to similar geometries. As these circuits become increasingly compact, parasitic capacitance between neighboring conductors becomes more problematic. Considerable effort has gone into developing numerical and analytical approximations that give reasonable estimates of the capacitance per unit length between nearby conductors (refs. 9, 10, and 11). Zahn (ref. 12) described a method valid for pairs of roughly rectangular conductors in close proximity on the same plane (fig. 14). The fringe field lines are approximated

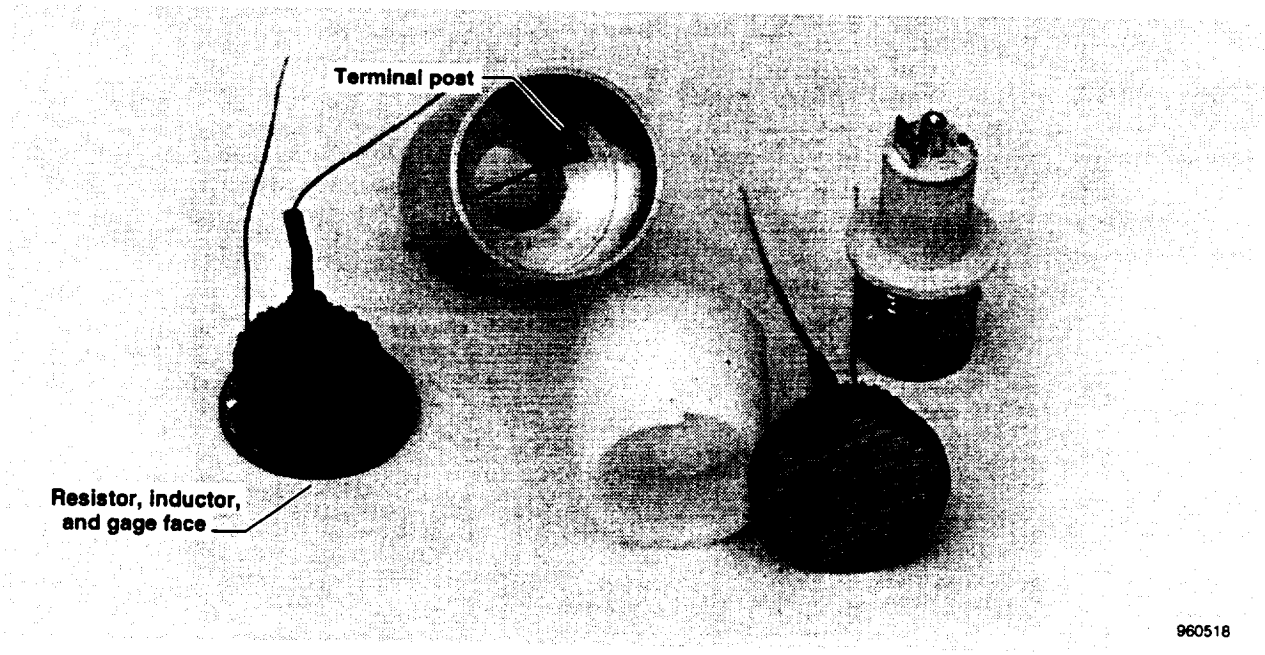

Figure 12. The 60 ... 10 gage geometry plus gage parts detail.

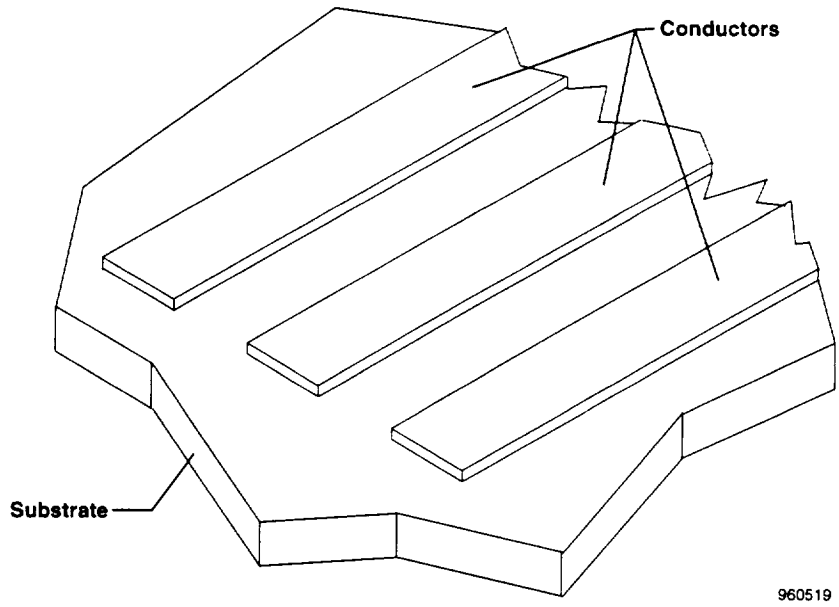

Figure 13. General gage face layout.

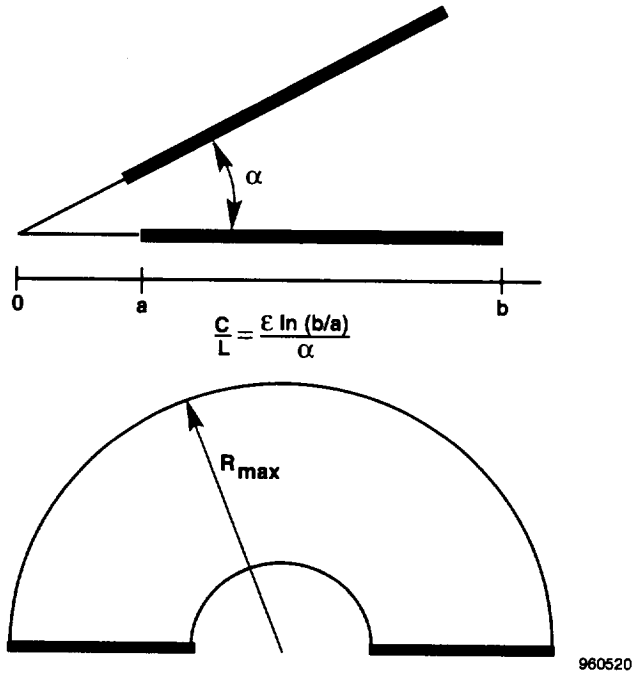

Figure 14. Zahn's method of approximating fringe field lines.

by semicircles and the capacitance per unit length is given by

$$C/L = \frac{\varepsilon \ln(b/a)}{\alpha} \qquad (2)$$

Equation (2) only estimates the fringing component. As the conductors or gaps become wider, the maximum semicircle radius grows. In this simplistic model, a gage geometry with wide conductors and gaps is sensitive to the presence of a dielectric further from its surface than a gage geometry with narrow conductors and gaps. This trend is evident in results from the finite-element analysis and lab tests, described in the following section.

Finite-Element Models

The two-dimensional, finite-element model of each configuration consists of the maximum conductors and gaps that can fit into a distance of 0.565 in. (14.35 mm), which is the inside diameter of the casings used in all the sensors tested. In some cases, the total width was ±0.565 in. (14.35 mm), but never deviated more than 0.010 in. (0.254 mm). Figure 15 shows a closeup of the mesh near some of the conductors for the 10/20 geometry (conductor width of 0.010 in. (0.254 mm) and gap width of 0.020 in. (0.508 mm)). From bottom to top, the model includes:

- The entire thickness of the PC-board
- The conductors themselves, which are represented by appropriate potential boundary conditions
- A filler between and slightly above the conductors
- Five successive layers of dielectric elements

The first three layers of elements are 0.010 in. (0.254 mm) thick, and the last two are 0.020 in. (0.508 mm) thick. These layers can be assigned either the permittivity of air or a dielectric (i.e., ablator). For instance, to simulate the presence of a dielectric 0.020 in. (0.508 mm) thick, the dielectric permittivity is assigned to the first two element layers above the probe and air permittivity to the remaining three. Thus dielectric thicknesses of 0, 0.010 in. (0.254 mm), 0.020 in. (0.508 mm), 0.030 in. (0.762 mm), 0.050 in. (1.27 mm), and 0.070 in. (1.778 mm) can be simulated. Because many of the geometries were apparently unsuitable for measuring dielectric thicknesses above 0.050 in. (1.27 mm), results are presented only for the dielectric range of 0 to 0.050 in. (1.27 mm).

The following is a note on nomenclature. The gage face geometries are designated by two or three numbers separated by a slash (/) or ellipsis (...). The first number is the conductor width in thousandths of an inch, while the second number is the gap width. For example, 20/10 indicates a conductor width of 0.020 in. (0.508 mm) and a gap width of 0.010 in. (0.254 mm). When three numbers are used, they indicate, in order, widths of the first plate conductor, gap, and second plate conductor. Serial numbers are also used to distinguish duplicate geometries. Table 1 lists the gage geometries and their corresponding serial numbers. The 60 ... 10 geometry is a design whose conductor widths vary from 0.060 to 0.010 in. (1.524 to 0.254 mm).

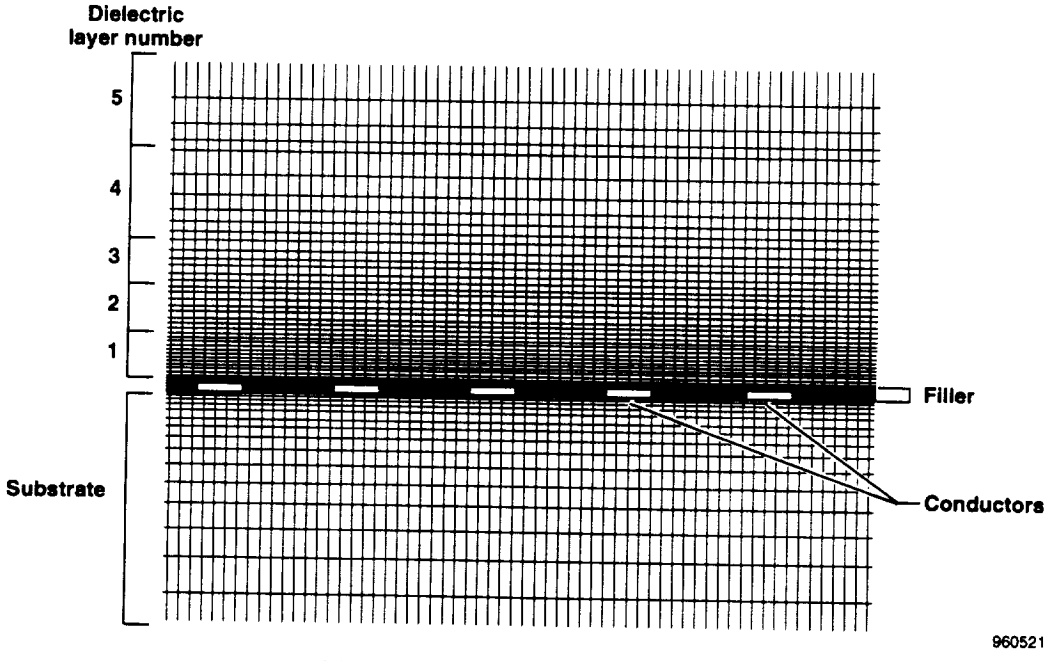

Figure 15. Typical mesh geometry.

Table 1. Gage geometries tested.

Serial number	Conductor/gap designation	Dry resonant freq., MHz
1	20/20	117
2	10/10	114
3	10/20	122
4	20/10/5*	130
5	20/20	124
6	20/10/10*	122
7	5/15	121
8	10/10	128
9	5/10	148
10	5/20	118
11	10/20*	117
12	20/10	132
13	40/40	93
14	40/40	95
15	40/40	98
16	40/40	97
17	40/40	98
18	30/30*	100
19	60/20*	113
20	60 ... 10*	120

*Geometries not modeled with finite elements.

An effort was made to standardize the finite-element models so that the effects of different conductor/gap geometries are accentuated. The models contain only the conductors and gaps of each configuration—not the widened areas near the edges that incorporate the soldered through-holes on the actual sensors—because these areas tend to be proportioned differently from gage to gage. No effort was made to incorporate the instrument casing; instead the PC board, filler, and all five dielectric layers are extended 0.050 in. (1.27 mm) past the end of the last conductor on each side. The computational elements nearest the conductors are a standard size independent of the configuration being modeled (0.0005 in. by 0.0025 in., or 0.0127 mm by 0.0635 mm). This choice of size allows a constant number of elements (four) along the vertical dimension of the conductors and some integer number along the horizontal dimension, depending on line width. Even the smallest line width (0.005 in. (0.129 mm)) has at least two elements along its horizontal dimension. The appendix gives an example of a geometry input file.

As discussed above, the probes are fabricated using two-sided PC board. The copper is left intact on most of the probe's back side except the two solder pads surrounding the through-holes. The finite-element model approximates this uncharged conductor as a boundary at zero potential (the lower edge of figure 15). Alternating conductors are assigned potentials of ±1 V. The remaining three boundaries (right, left, and top) of the mesh are truncated with so-called absorbing boundary conditions (ABCs) (ref. 13) to approximate regions extending to infinity. Open region problems can require many mesh nodes, but ABCs appear to allow efficient, accurate truncation of meshes much nearer the structure of interest.

The governing equation for electrostatic analysis in the presence of dielectrics is

$$\nabla \cdot \varepsilon \nabla V = -\rho \tag{3}$$

where ρ is the charge density and V is the potential difference. The code solves for the electric field, displays the potential map, and calculates the stored energy. The capacitance of the geometry (in pF/cm normal to the plane) is found from

$$C/L = \frac{2E}{V^2} \tag{4}$$

where E is the stored electrical energy per unit length. Figures 16 and 17 are two views of the output from the 10/20 geometry. Shaded areas represent ranges of potential, with interfaces between different shades representing curves of constant potential. Figure 16 depicts about half the problem domain, while figure 17 is a closeup. Figures 16 and 17 show elements above the gage surface up to a distance of 0.050 in. (1.27 mm) that are assigned a dielectric constant of 3 (representative of an ablator). Figure 18 depicts the case when no ablator is present. Note (fig. 18) how the curves of constant potential lie farther above the conductor surfaces when compared with the case for the ablator.

Recall the basic parallel plate capacitor. When a material with a higher permittivity than air is placed between the plates, the capacitor can store more energy at a given voltage, that is, its capacitance increases. To see this happening more clearly for the geometries analyzed here, figures 19 through 22 plot capacitance

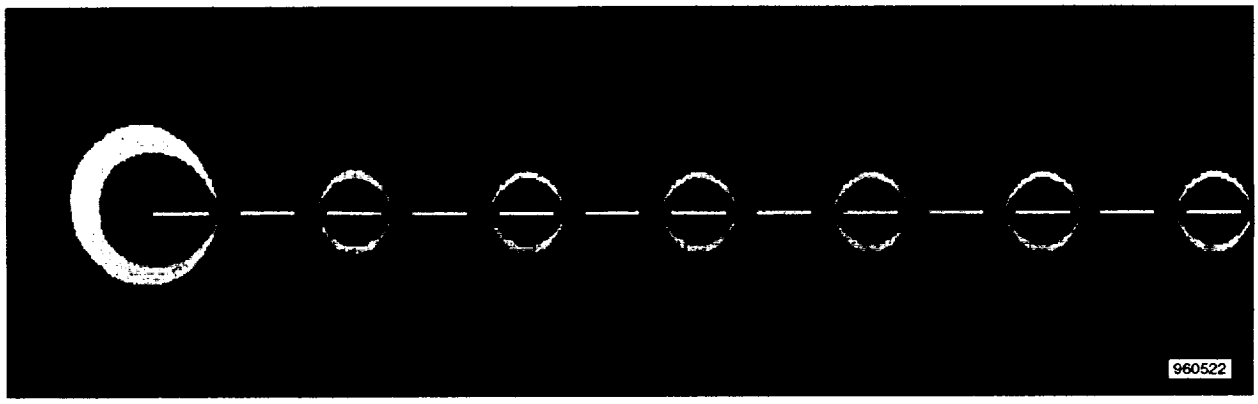

Figure 16. Potential regions for 10/20 geometry; ablator thickness = 0.

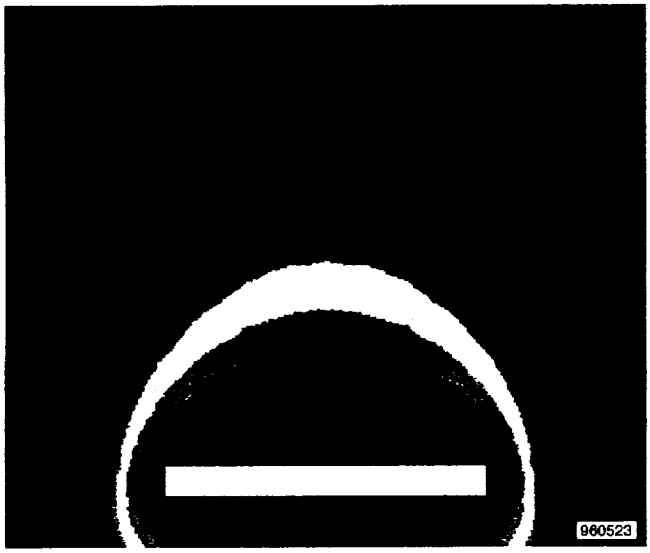

Figure 17. Closeup of potential regions around 10/20 geometry; ablator thickness = 0.

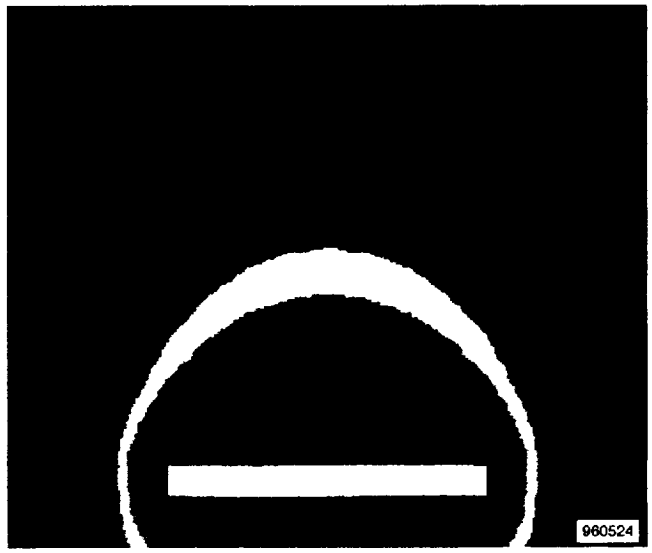

Figure 18. Closeup of potential regions around 10/20 geometry; ablator thickness = 0.050 in. (1.27 mm).

(in picofarads per centimeter) as a function of ablator thickness. The slopes between five data points are indicated for each gage geometry. As expected, every gage geometry is most sensitive (i.e., steep slope) to changes in ablator thickness between 0 and 0.010 in. (0.254 mm) and least sensitive to changes in ablator thickness between 0.030 and 0.050 in. (0.762 and 1.27 mm). This result indicates how the gage output varies as the dielectric thickness changes.

When comparing different geometries, the percentage change in capacitance is important. For instance, as the gaps become wider (fig. 19) for a fixed conductor width of 0.005 in. (0.127 mm), the capacitance as a function of ablator thickness becomes more linear; that is, there are lower slopes for the thin ablator thicknesses and higher slopes for the thicker ablator thicknesses. Note, however, that the capacitance level per unit length goes down as the gap width increases. Comparing the 5/10 and 5/20 geometries in figure 19, the 5/20 geometry seems to be less sensitive to ablator thicknesses between 0 and 0.010 in. (0.254 mm) because its slope in this region is less than half of that for the 5/10 geometry. However, the capacitance change over this region is roughly the same percentage for both geometries.

For ablator thicknesses between 0.030 to 0.050 in. (0.762 and 1.27 mm), the 5/20 geometry's higher slope and lower level combine for a larger percentage change in capacitance in this region than the 5/10 geometry. The trends continue for conductor widths of 0.010 in. (0.254 mm), 0.020 in. (0.508 mm), and 0.040 in. (1.016 mm) shown in figures 20, 21, and 22. Figure 23 summarizes gage average sensitivities (ΔpF/cm)/(mm dielectric) for dielectric thicknesses between 0.030 and 0.050 in. (0.762 and 1.27 mm). Over this range of dielectric thickness, the 40/40 configuration's sensitivity is almost two orders of magnitude larger than that for the 5/10 geometry.

GAGE TESTING

Testing was divided into two phases, which were both conducted under room temperature conditions. The first phase involved bench-testing the candidate gages using an ablator substitute. During this phase, the ablator was simulated by Delrin shims machined to various thicknesses. The results of phase 1 testing consist of a single curve of RCB output as a function of shim thickness for each probe.

The second phase involved flush-mounting the gages to an aluminum plate and applying an ablator in a layer of suitable thickness. The ablator was sanded off to produce a single curve of RCB output as a function of ablator thickness for each gage.

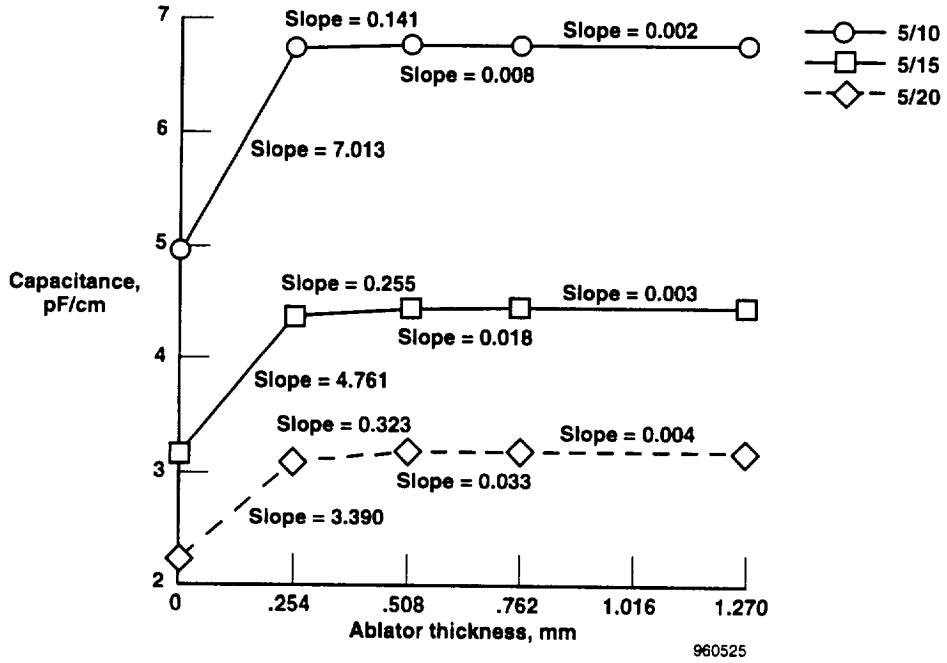

Figure 19. Electrostatic code results; capacitance as a function of ablator thickness; conductor widths = 0.005 in. (0.127 mm).

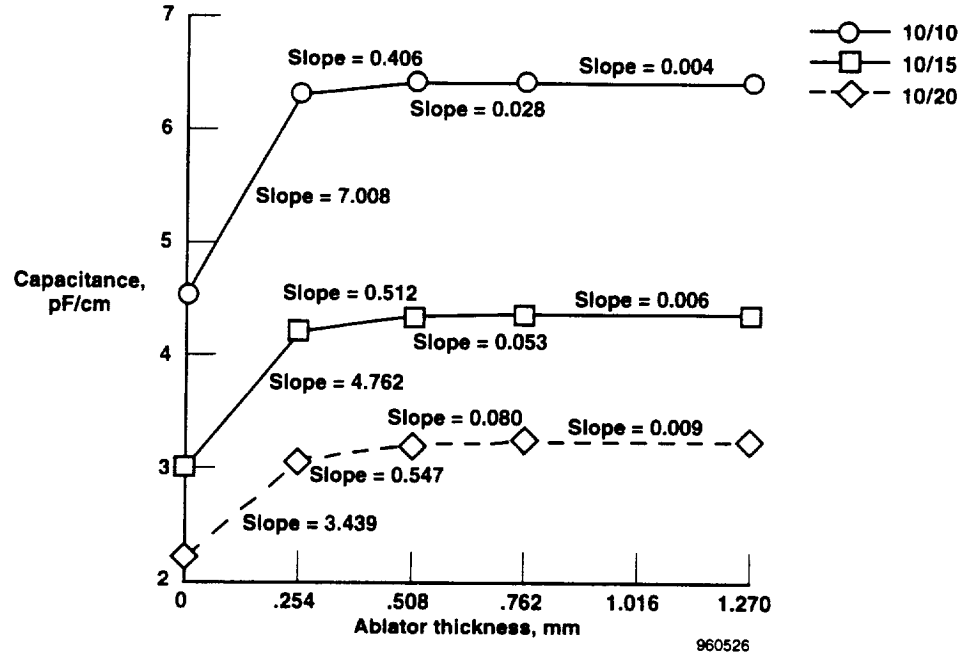

Figure 20. Electrostatic code results; capacitance as a function of ablator thickness; conductor widths = 0.010 in. (0.254 mm).

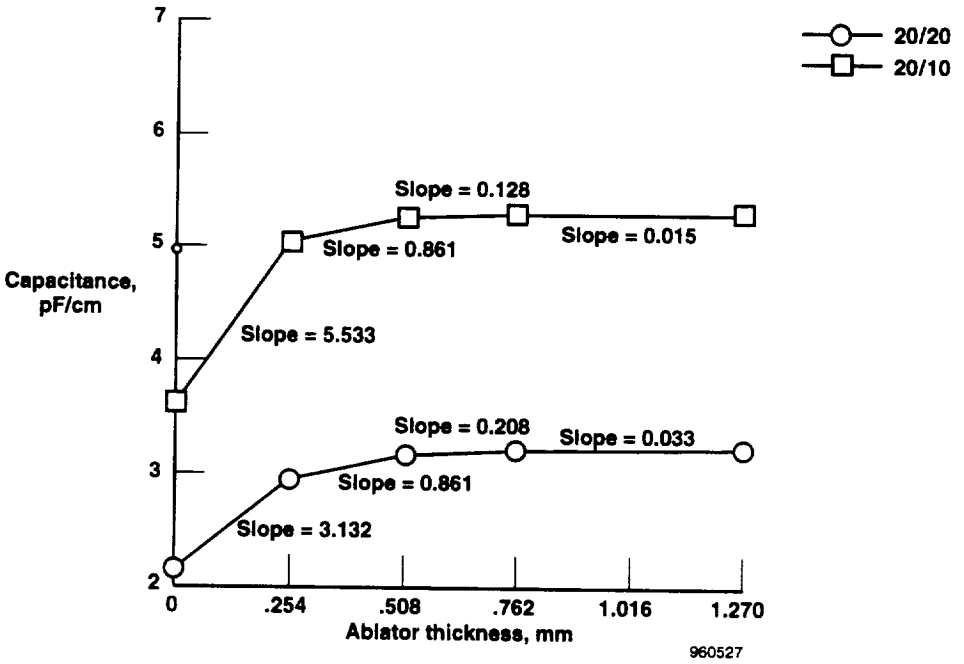

Figure 21. Electrostatic code results; capacitance as a function of ablator thickness; conductor widths = 0.020 in. (0.508 mm).

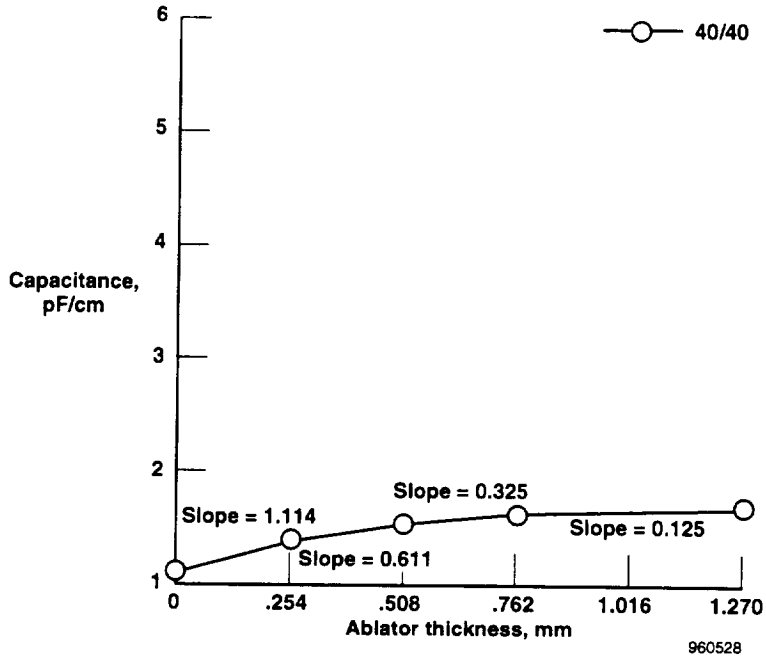

Figure 22. Electrostatic code results; capacitance as a function of ablator thickness; conductor widths = 0.040 in. (1.016 mm).

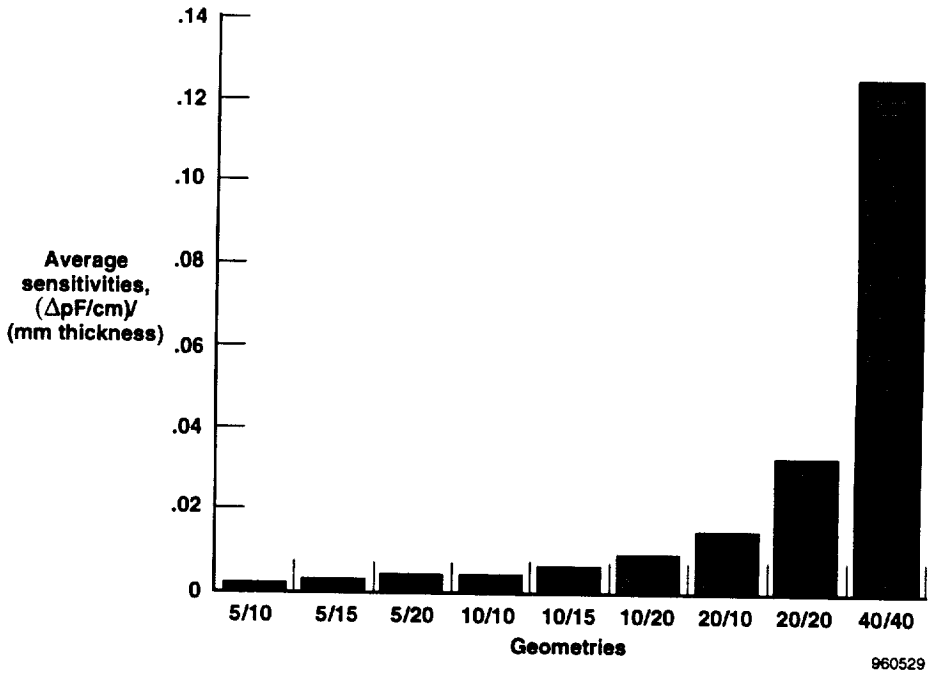

Figure 23. Summary of electrostatic code results.

The phase 1 procedure follows:

1. Set up the oscillator/RCB/gage circuit as shown in figure 7, using an ordinary voltmeter to monitor RCB output.
2. With nothing on the face of the gage, vary the frequency of the signal generator until the minimum RCB output is noted on the voltmeter.
3. Apply Delrin shims of different thicknesses while recording the output of the RCB. Take care that each shim is placed in the same axial orientation with respect to the gage. Careful placement ensures that each gage is measuring the same part of a possibly warped or uneven shim.
4. Repeat steps 1 through 3 for all of the remaining gages.

Phase 2 testing involved placing four gages into a test fixture with an ablator covering them. The fixture was built to allow accurate measurement of ablator thickness over each gage using a dial indicator (fig. 24). A two-component, commercially available ablator (ref. 14) was applied in liquid form. (Thermal properties include ρ_m = 1440 kg/m^3, k = 0.138 W/m · K, c_p = 1248 J/kg-K). Aside from the requirements of dealing with an actual ablator, phase 2 procedures were similar to those in phase 1.

The phase 2 procedure follows:

1. Mount four gages at a time flush with the surface of the test fixture.
2. Set up the signal generator/RCB/voltmeter system as in phase 1 (fig. 7). Connect the termination side of the RCB to only one gage at a time.
3. For each gage in turn, vary the signal generator frequency to find the minimum RCB output.
4. Zero the dial indicator over each bare fixture.
5. Apply a layer of ablator over the fixture and gages to a depth of about 0.10 in. (2.54 mm). Allow the ablator to cure.
6. Record the depth of ablator over the face of each gage, using the dial indicator.
7. Record the RCB output for all gages in turn, while taking care to return the signal generator to the proper frequency for each gage found in step 3.
8. Remove a layer of ablator. Repeat steps 6 and 7.

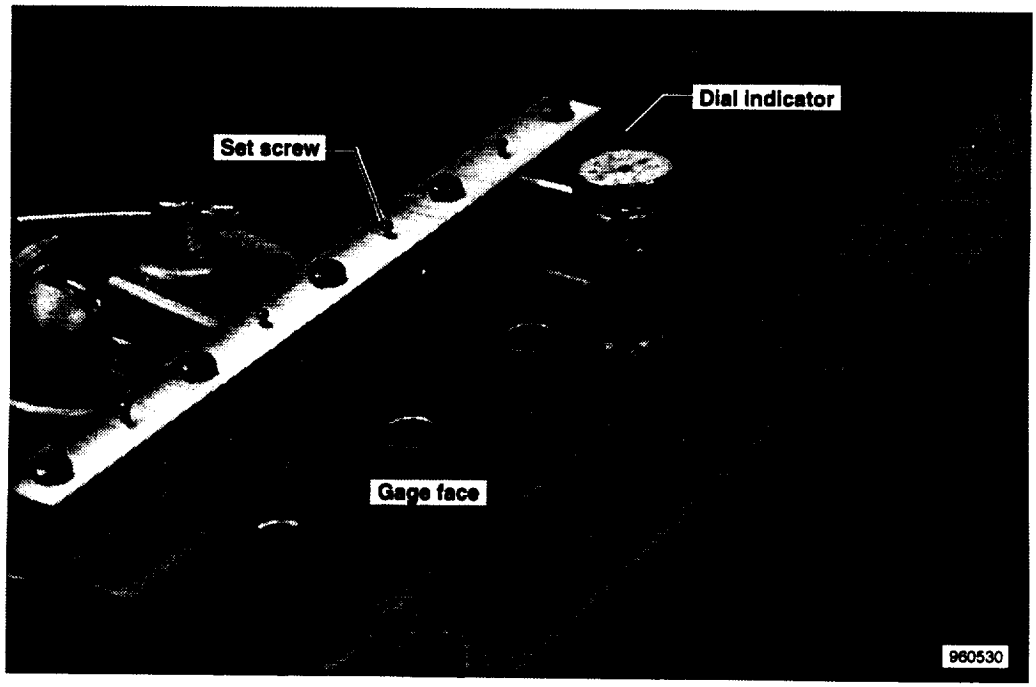

Figure 24. Closeup of gage test panel for phase 2 testing.

Results of Phase 1 Testing of the Initial 12 Gages

Figures 25 through 29 depict RCB output as a function of shim thickness from the initial 12 candidate geometries. Most graphs appear jagged because some shims had uneven thicknesses and some were warped after manufacture. If a shim was warped, part of it rode above the gage surface, lowering output. Compounding the problem was the solder through-holes on the 12 gages. Often, a small bead of solder formed and protruded slightly above the gage surface. If a flat shim was placed on such a gage, it rode slightly above the gage surface thus lowering gage output. While these defects prevented us from attaining a smooth, one-to-one correspondence between RCB output and dielectric shim thickness, they were repeatedly detected by most gages. For instance, the third-largest shim, 0.050 in. (1.27 mm) (the third data point from the right on all the graphs), returned a lower RCB output than either of its neighbors on most gages in figures 25 through 29. The same statement can be made about the 0.039-in. (0.991-mm) shim (the fifth data point from the right).

Maximum RCB output ranged from less than 10 mV (5/10, fig. 25) to more than 200 mV (20/20, fig. 29). Generally, the higher the gage capacitance (narrow lines and gaps), the lower the maximum output and the lower the sensitivity or slope. Based on the finite-element analysis described earlier, we expected a lower maximum output for these gages. Over the entire dielectric range, capacitance increased by about 36 percent for the 5/10 geometry and by about 50 percent for the 20/20 geometry (figs. 19 and 21). Recall that for narrow line or gap geometries, a larger percentage change occurs over the thickness range of 0 to 0.010 in. (0.254 mm) than for wide line or gap geometries. Thus, if a shim rides above the gage surface because of warping or the presence of solder beads, it lowers the output of the gages with narrow line or gaps more severely than the output of gages with wide line or gaps.

The shim tests of the initial 12 gages verified the trends evident in the finite-element analysis and predicted by Zahn's fringe field approximation; that is, wider line or gap geometries are more sensitive to the thicker layers of dielectric or ablator. With this lesson learned and the fabrication experience of the first 12 gages in mind, we designed and constructed 8 more gages. The new geometries included a 30/30, a 60 ... 10, a 60/20, and five 40/40s. Figure 12 shows the 60 ... 10 gage before assembly.

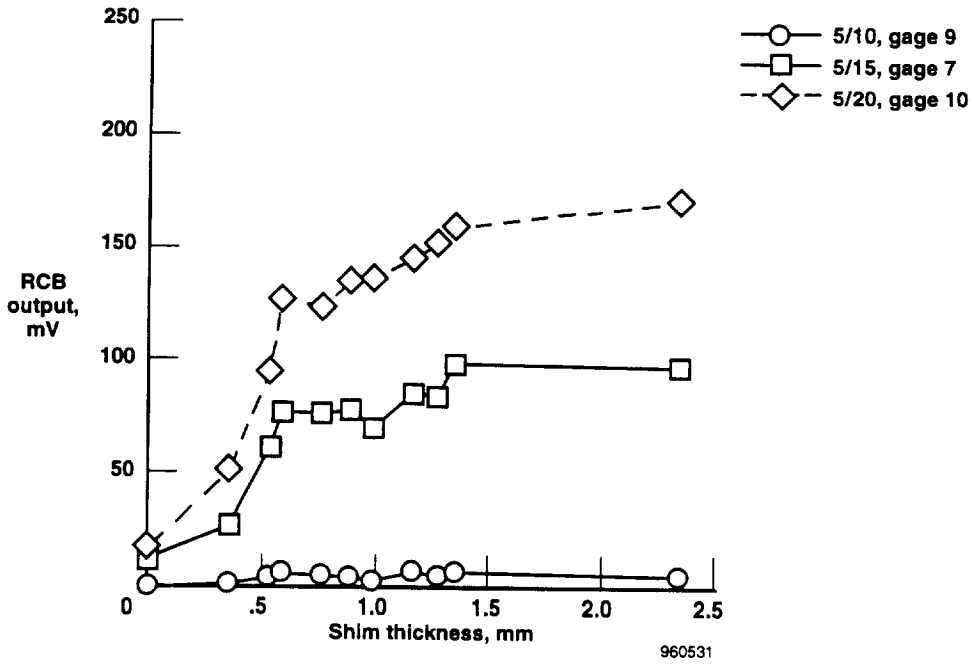

Figure 25. Shim test results; RCB output for gage geometries 5/10, 5/15, and 5/20.

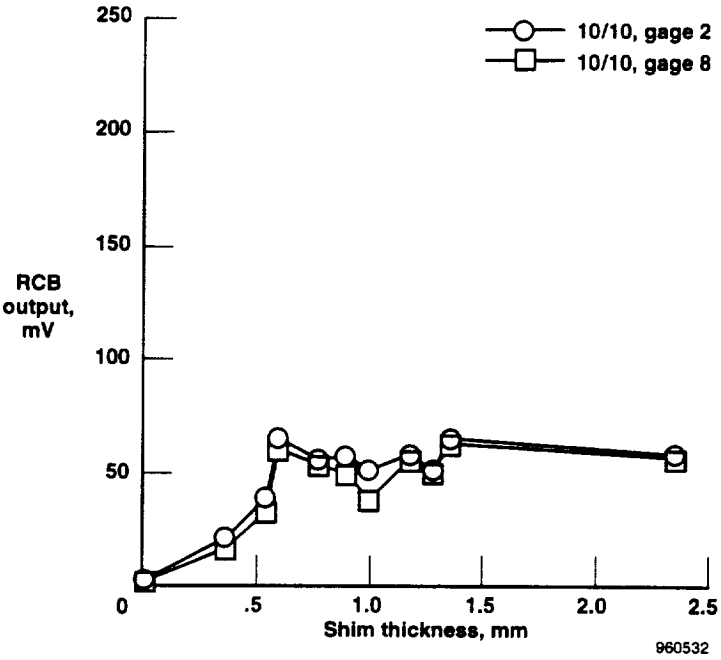

Figure 26. Shim test results; RCB output for gage geometry 10/10 (sensors 2 and 8).

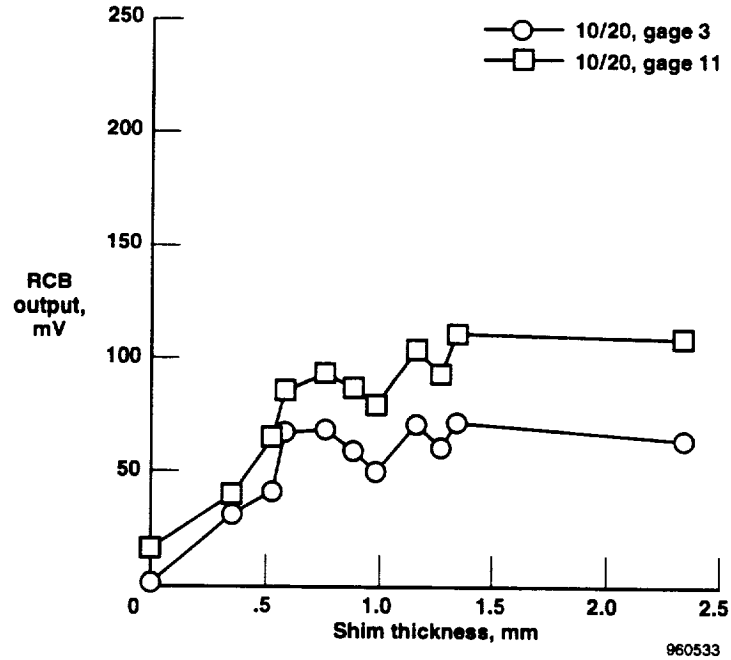

Figure 27. Shim test results; RCB output for gage geometry 10/20 (sensors 3 and 11).

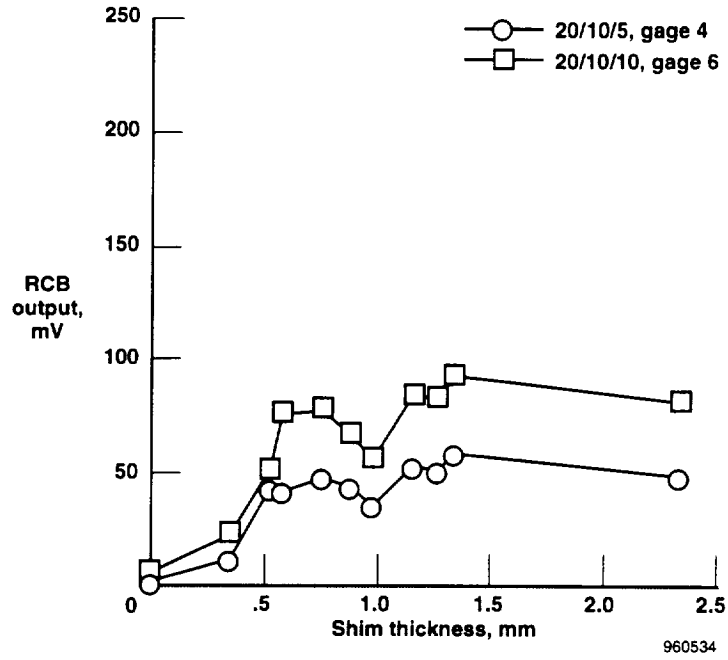

Figure 28. Shim test results; RCB output for gage geometries 20/10/5 and 20/10/10.

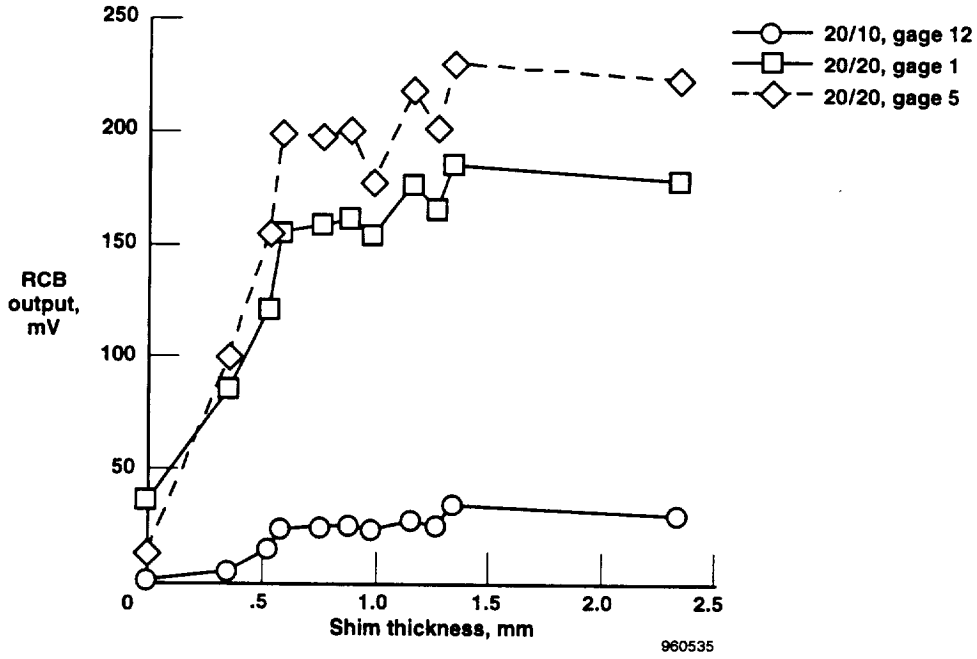

Figure 29. Shim test results; RCB output for gage geometries 20/10 and 20/20 (sensors 1 and 5).

Figures 30 through 33 depict results of the shim tests for the last eight gages. Note the change in scale compared with the plots for the first 12 gages. Maximum output is more than 400 mV (sensor 15 and 16, fig. 31) compared with 200 mV for the first 12 gages tested. For the 40/40 and 30/30 gages (figs. 30 through 32), RCB output has nearly a one-to-one correspondence with shim thickness through the third-largest shim, in particular for sensors 13 and 15. The 30/30 gage output (sensor 18, fig. 32) appears a bit more jagged than that for the 40/40 gages and has a lower maximum of about 360 mV. The 60/20 gage (sensor 19, fig. 33) performs very similarly to the 30/30 only with a lower zero and a maximum of about 350 mV.

All gages from 13 to 19 have high outputs compared with the initial 12 gages, and all have discernible, positive slopes out to the thickest (0.092 in. or 2.337 mm) shim. The 60 ... 10 geometry fared more like its predecessors but no worse than the 20/20 geometries. The 60 ... 10 gage resonated at the target frequency of 120 MHz and had a very small zero reading.

Results of Phase 2 Testing

Phase 2 testing was performed on four gages of the 40/40 geometry (sensors 13 through 16). Figure 34 shows the results. Note that the zero thickness output for all four gages was virtually the same as their respective zeros for the shim tests of phase 1 (figs. 30 and 31). In the shim tests of phase 1, the gages were held upright by their coaxial cables, not mounted in an aluminum plate as in phase 2. Unchanging zeros between the two tests demonstrate that the gages are properly shielded and are indifferent to the method of mounting. The gages, however, must be electrically isolated from their mounting.

Maximum outputs for the phase 2 tests were about 200 mV higher than for the phase 1 shim tests. Delrin (acetal) and the ablator have similar dielectric constants (≈ 3), but the rigid shims of phase 1 rested on top of the conductors while the ablator of phase 2, applied in liquid form, occupied the volume directly between the plates of the capacitors. The presence of ablator material in the most sensitive region of the gage resulted in a large output even when very little material remained above the conductors. This large initial jump tended to wash out the response to thicker layers of material. Nevertheless, one can still see a discernible slope at the thicker layers and similar curves to those generated by the shim tests, particularly for sensors 15 and 16.

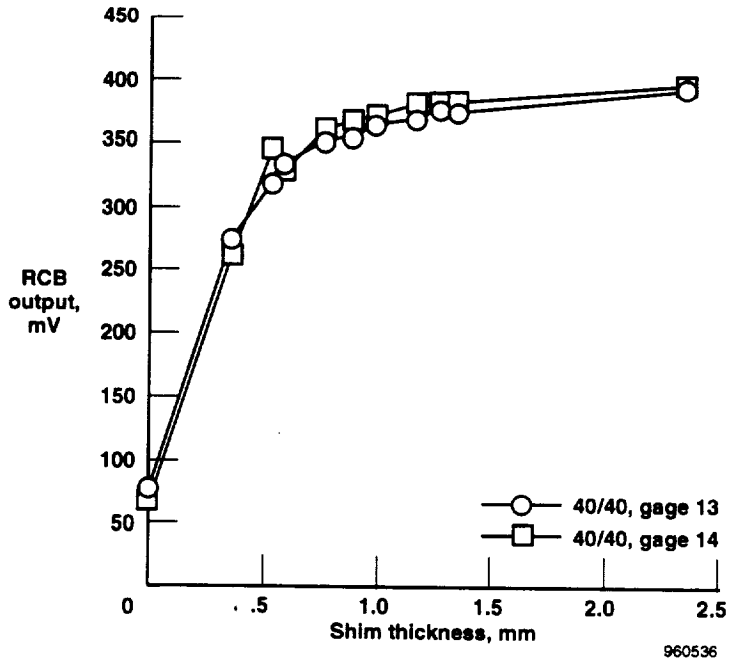

Figure 30. Shim test results; RCB output for gage geometry 40/40 (sensors 13 and 14).

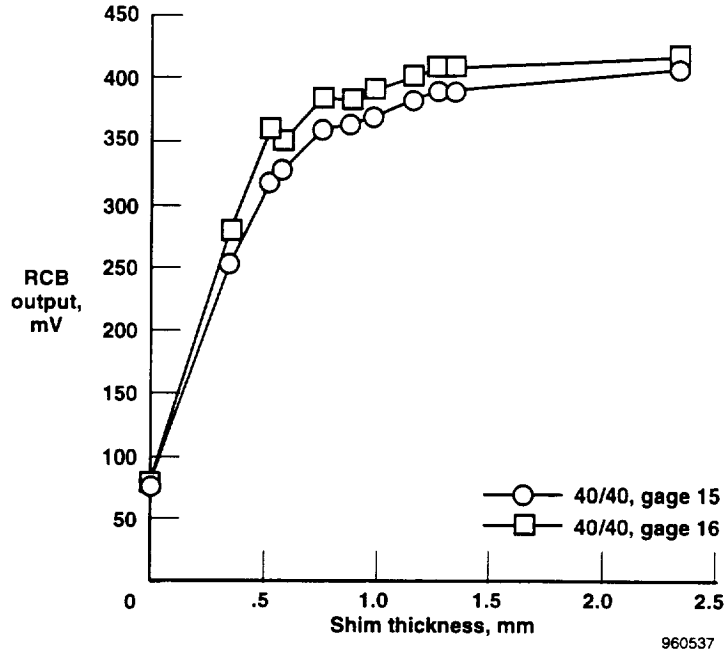

Figure 31. Shim test results; RCB output for gage geometry 40/40 (sensors 15 and 16).

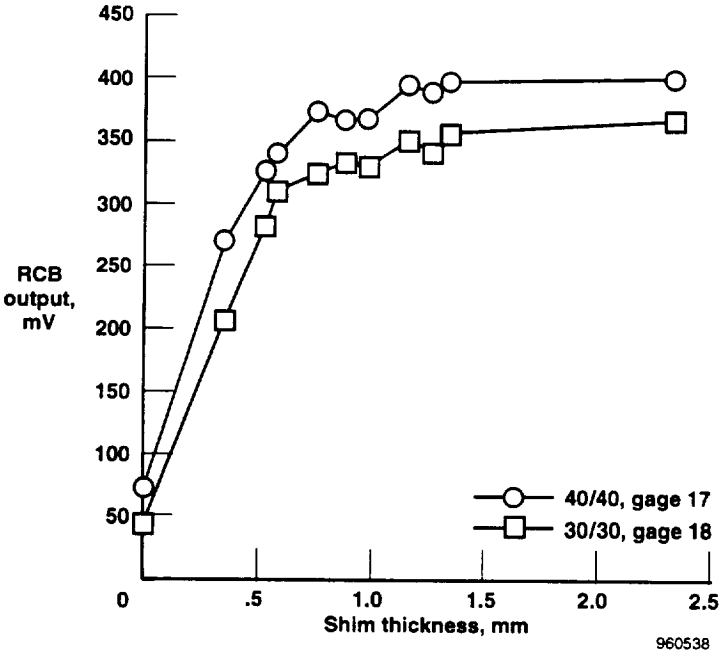

Figure 32. Shim test results; RCB output for gage geometries 40/40 (sensor 17) and 30/30 (sensor 18).

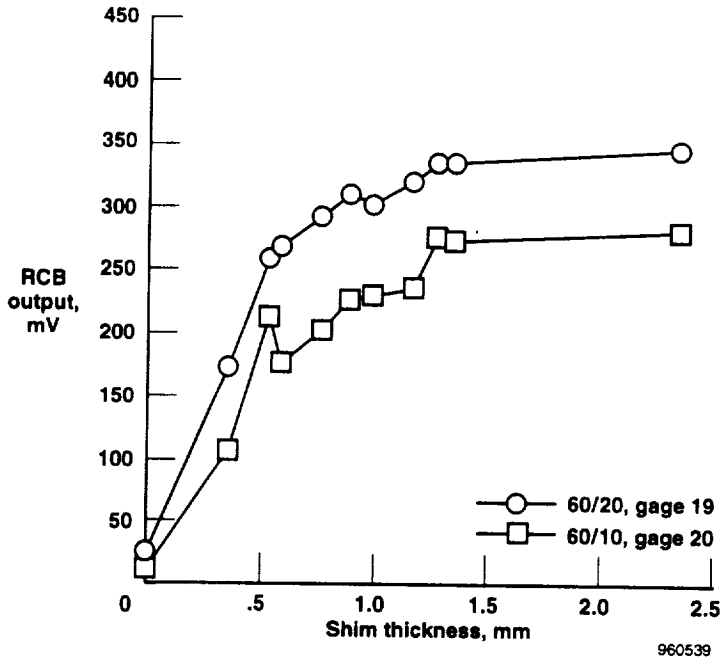

Figure 33. Shim test results; RCB output for gage geometries 60/20 and 60 ... 10.

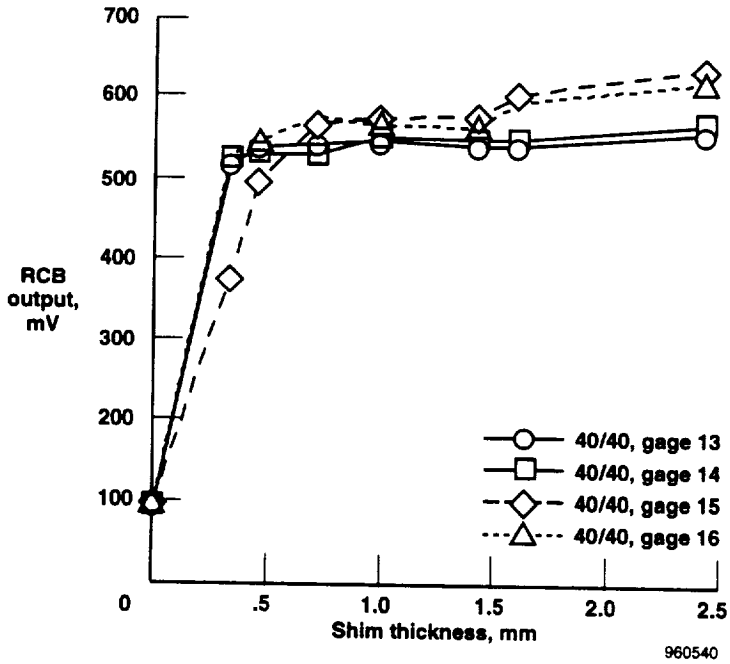

Figure 34. Ablator test results; RCB output for gage geometry 40/40 (sensors 13, 14, 15, and 16).

DISCUSSION

The primary lesson learned is the effect of gage geometry on sensitivity. Finite-element analyses, analytical approximations, and test results all indicate that wider lines and gaps increase sensitivity to material above the conductors and increase the range of material thicknesses that can be quantified. Wider lines and gaps also lead to lower gage face capacitances, thus increasing the effect of stray capacitance or inductance in the rest of the gage and making it harder to produce a tuned gage using the fabrication method described here. Because future designs will incorporate wide lines and gaps, a method of tuning the gage after final assembly is required. Small, tunable capacitors and inductors are commercially available (ref. 15) and could be integrated into the RLC termination.

In the present method of fabrication, the gage face, inductor, resistor, and Delrin chassis are placed in the front casing. Three lead wires (one each from the inductor, resistor, and casing) protrude from the casing's back. The inductor and casing leads are soldered to the shield side of the BNC and the resistor lead is soldered to the other pin. Potting is forced into the back of the casing and air bubbles are given time to escape. The BNC is then simply pressed into the casing's back, doubling over the lead wires connected to it. Future designs should incorporate a BNC mounted so that the axis of the BNC is parallel to the gage face. Access to the casing's back should allow soldering of lead wires without having to double them over as the BNC is inserted. This design would further cut down on stray capacitances and allow access to a tunable capacitor or inductor.

All gages described here are compact and mechanically stable, and some accurately measure the thickness of dielectric materials placed above them. All, however, are unsuitable for working in high-temperature ($\approx$ 120 °C) environments. As mentioned earlier, the nonhomogeneous construction of the gage (i.e., printed circuit board, Delrin chassis, and potting with possible air bubbles) make accurate thermal modeling very difficult. In addition, the fiberglass circuit board and potting are not intended for use at these temperatures. A homogeneous substructure is needed that has known thermal properties and high-temperature capability.

A technique used for depositing metallic traces on high-temperature substrates, such as quartz and Macor®, using "organo-metallic" materials could prove useful. The line or gap geometry of a capacitive gage would be placed on a substrate of sufficient thickness to allow simple thermal modeling and protection for the associated electronic components. The thickness of the traces is significantly thinner (on the order of microns) than traces etched on PC board, further reducing the parallel plate component and eliminating the problem of a large initial jump in output when a material is sprayed or poured on without a coating.

Although the signal generator used for this test, and shown in figure 7, can generate a wide range of frequencies, the gages are intended to resonate close to the same frequency ($\approx$ 120 MHz) in anticipation of using a much smaller crystal oscillator that is only slightly adjustable. Recall that after a gage's capacitance is fixed, its resonant frequency is primarily controlled by the number of turns on the inductor. From equation (1), for a given frequency, a lower capacitance gage requires a larger inductance (i.e., more turns). For the toroidal cores used in these gages, the required number of turns is quite small, varying between about 13 and 23. In practice, all the wires within the gage contribute to the inductance and capacitance so the number of turns derived from equation (1) and the core manufacturer's specifications is only a rough estimate, and the number of turns must be adjusted before final assembly.

Table 1 summarizes the resonant frequency for all the gages. While some resonated very close to the desired 120 MHz, many did not, and several tactics were attempted to remedy the situation. These tactics included using thick-walled silicon tubing around some of the internal wires to keep them from coming too close to one another after final assembly and lengthening the sensor case to prevent wires from doubling over. The entire ordeal demonstrated the need for the ability to tune the gage after final assembly.

Phase 2 testing solved some problems from the shim tests but brought up new ones. The question of warped material was eliminated; because the material was poured in liquid form, continuous contact was ensured with the gage surface. As the material was removed by sanding with a flat sanding block, however, two problems arose. First, although care was taken to remove an even layer of ablator between data points, measurements indicated that the thickness of material removed

® Macor is a trademark of Corning Glass, Corning, New York.

varied for different gage locations. These variations were minimal, and a constant material thickness can be assumed over each gage face without too much error. Second, small voids (< 0.4 mm) became exposed and tended to pack with the sanding residue. Vacuuming removed the residue from most voids but left the smallest ones packed. A higher output than expected resulted after a layer of given thickness was removed.

Although eventually necessary for every new design, testing with the actual ablative material is inherently messy. Fortunately, most problems associated with phase 2 testing (i.e., ablator material between the conductors, uneven thickness above the gages, and the presence of voids) seem avoidable. First, if a dielectric material, for instance a common circuit board coating is placed on the gage face, the ablator material cannot get into the interplate region. Any material poured or sprayed over the gage acts more like the rigid shims of phase 1. Recall that this is how the finite-element models were set up. Care should be taken to find a suitable material with as low a dielectric constant as possible. If the organo-metallic technique described earlier or a similar deposition method is used, thinner conductor traces will result and the between-plate volume is significantly reduced to begin with.

Second, the problem of uneven material removal can be solved if the entire test fixture is placed in a milling machine and the ablator simply machined off. The ablator material used in this test exhibited fine mechanical properties (it sanded much like a soft wood filler). If a different material is used, these characteristics would have to be demonstrated first. A thicker test panel (i.e., about 1 to 1.5 cm) would also be required to increase rigidity. Third, if the ablator material is mixed and allowed to settle for about an hour in a sealed container (curing time is about 12 hr after the volatiles are allowed to evaporate) before application, most small bubbles from the mixing of components dissipate. This additional step, along with the use of a milling machine, helps to alleviate the void-packing problem.

CONCLUSIONS

A capacitive sensor concept that can nonintrusively measure the thickness of dielectric materials was developed for measuring ablator thicknesses on boost vehicles. Twenty capacitive gages with 13 sensing element geometries were fabricated and tested. A two-dimensional finite-element analysis was performed on several geometries. Calibration procedures using an ablator, as well as ablator-simulating shims, are described.

1. Through design and fabrication iterations, a capacitive gage concept that can nonintrusively measure the thickness of an adjacent dielectric shim was demonstrated. A one-to-one correspondence between system output and dielectric thickness was attained to dielectric thicknesses of about 0.055 in. (1.4 mm) for the ablator-simulating shims. The permittivity of the material was about three times that of air or vacuum. Changes in designs, calibration procedures, and fabrication techniques are suggested to improve this performance. These changes include (a) using organo-metallic or other techniques to deposit conductors on a high-temperature substrate, (b) using a tunable capacitor to force all gages to resonate at a given frequency, and (c) using machine tools to remove ablator material during laboratory tests in lieu of hand sanding.

2. Gages with wide conductors and gaps are sensitive to a dielectric further from their surfaces than gage geometries with narrow conductors and gaps. This finding was verified by a finite-element analysis and laboratory tests, and is consistent with an analytical approximation.

3. Minimizing the parallel plate component of capacitance by decreasing the thickness of the conductors is necessary to increase sensitivity to useful levels. This finding was demonstrated by the success of 20 PC board gages relative to the gage constructed of machined brass rings. Reducing the parallel plate component further over the PC board gages by using the fabrication techniques described in this technical memorandum would improve gage performance when an ablator is applied in liquid form (as in phase 2 testing) and might eliminate the need for a permanent coating.

4. A novel system circuitry was developed that (a) gives a high-level output, (b) is insensitive to cable position and outside noise, and (c) isolates the capacitance being measured to the sensor itself. This circuitry represents a significant improvement over past designs intended for

thin-film measurement that integrated the gage capacitance into a frequency modulation circuit.

5. The more sensitive, wide conductor or gap gages have a lower gage face capacitance and are more easily affected by stray capacitances within the body of the resistive, inductive, and capacitive termination (i.e., gage casing). This design makes it more difficult to have different gages resonate at the same frequency using the present untunable designs. If different gages can be made to resonate at an equal frequency, they can be excited by a fixed-frequency crystal oscillator.

6. Wiring the gage casing to the shield side of the incoming coaxial cable provided adequate shielding and eliminated the sensitivity of the gage to its mounting arrangement.

Dryden Flight Research Center
National Aeronautics and Space Administration
Edwards, California, July 2, 1996

REFERENCES

1. Legendre, Phillip J., "Reentry Vehicle Nosetip Instrumentation," *Proceedings of the 22nd International Instrumentation Symposium,* San Diego, California, 1975.

2. Hycal Engineering, "In-Depth Ablative Plug Transducers," Series #S-2835, 9650 Telstar Avenue, P. O. Box 5488, El Monte, California, 1992.

3. Armini, A.J. and S.N. Bunker, "A Re-entry Vehicle Nosetip Shape Change Sensor," *Proceedings of the 21st International Instrumentation Symposium,* Philadelphia, Pennsylvania, 1975.

4. McGunigle, Richard D. and Michael Jennings, "Ultrasonic Ablation Recession Measurement System," *Proceedings of the 21st International Instrumentation Symposium,* Philadelphia, Pennsylvania, 1975.

5. Brown, Robert C., Paolo Andreussi, and Severino Zanelli, "The Use of Wire Probes for the Measurement of Liquid Film Thickness in Annular Gas-Liquid Flows," *The Canadian Journal of Chemical Engineering*, vol. 56, Dec. 1978, pp. 754–757.

6. Benn, D.N., "An Experimental Capacitance Liquid Film Thickness Monitor, Operating Instructions and Circuit Details," United Kingdom Atomic Energy Authority Research Group Report, Atomic Energy Research Establishment, Harwell, Berkshire, 1972.

7. Noffz, Gregory K., Robert E. Curry, Edward A. Haering, Jr., and Paul Kolodziej, *Aerothermal Test Results From the First Flight of the Pegasus® Air-Launched Space Booster,* NASA TM-4330. Oct. 1991.

8. Structural Research and Analysis Corp., COSMOS/M Version 1.71, "Basic FEA System User Guide, Part 1," vol. 3, 2951 28th Street, Suite 1000, Santa Monica, California, May 1994.

9. Ruehli, Albert E. and Pierce A. Brennan, "Capacitance Models for Integrated Circuit Metallization Wires," *IEEE Journal of Solid-State Circuits*, vol. SC-10, no. 6, Dec. 1975.

10. Ruehli, Albert E., "Survey of Computer-Aided Electrical Analysis of Integrated Circuit Interconnections," *IBM Journal of Research and Development*, vol. 23, no. 6, Nov. 1979.

11. Shrivastava, Ritu and Kelly Fitzpatrick, "A Simple Model for the Overlap Capacitance of a VLSI MOS Device," *IEEE Transactions on Electronic Devices*, vol. ED-29, no. 12, Dec. 1982, pp. 1870–1875.

12. Zahn, Marcus, *Electromagnetic Field Theory: A Problem Solving Approach,* New York, Wiley, 1979, pp. 272–273.

13. Khebir, A., A.B. Kouki, and R. Mittra, "An Absorbing Boundary Condition for Quasi-TEM Analysis of Microwave Transmission Lines via the Finite Element Method," *Journal of Electromagnetic Waves and Applications*, vol. 4, no. 2, 1990, pp. 145–157.

14. Charwat, A.F., "Exploratory Studies on the Sublimation of Slender Camphor and Naphthalene Models in a Supersonic Wind Tunnel," Memorandum RM-5506-ARPA (AD-673531), July 1968.

15. Johanson Manufacturing Corp., "Thin-Trim® and Seal-Trim® Trimmer Capacitors," Rockaway Valley Road, Boonton, New Jersey, n.d.

APPENDIX: FINITE-ELEMENT GEOMETRY INPUT

```
C*
C*    COSMOS/M      Geostar V1.70
C*    Problem : 2010          Date : 5-SEP-93
C*
C*    This problem will calculate the total stored energy in the
C*    20.10 geometry (from which capacitance can be derived). No
C*    solder pad effects are included.
C*
C*    ASSIGN THE WORKING PLANE AS X-Y, AND VIEW AS THE X-Y PLANE,
C*    AND, SCALE THE PICTURE UP ONCE.
PLANE,Z,0,1,
VIEW,0,0,1,0,
SCALE,0,
C*
C*    CREATE PARAMETRIC VARIABLES FOR THE MODEL GEOMETRY, AND
C*    ASSIGN VALUES.
C*    INCHES TO METERS CONVERSION FACTOR. (FEM MODEL IS 10X)
PARASSIGN,CONFAC,REAL,.254,
C*
C*    THICKNESS VARIABLES FOR THE REPEATING LINE AND GAP.
PARASSIGN,TLINE,REAL,.020*CONFAC,
PARASSIGN,TGAP,REAL,.010*CONFAC,
C*
C*    THICKNESS VARIABLES FOR CONDUCTORS, PCBOARD,
C*    FILLER,EDGES AND THE LAYERS OVER THE GAGE. THE LAYERS
C*    WILL BE ASSIGNED PERMITTIVITIES LATER, THUS DETERMINING
C*    THE THICKNESS OF THE ABLATOR
PARASSIGN,TL1,REAL,.01*CONFAC,
PARASSIGN,TL2,REAL,.01*CONFAC,
PARASSIGN,TL3,REAL,.01*CONFAC,
PARASSIGN,TL4,REAL,.02*CONFAC,
PARASSIGN,TCOND,REAL,.002*CONFAC,
PARASSIGN,TPC,REAL,.063*CONFAC,
PARASSIGN,TAIR,REAL,.02*CONFAC,
PARASSIGN,TFIL,REAL,.0025*CONFAC,
PARASSIGN,TEDG,REAL,.05*CONFAC,
C*
C*    DEFINE MATERIAL PROPERTY SETS
MPROP,1,PERMIT,17.7E-12,
MPROP,2,PERMIT,8.65E-12,
MPROP,3,PERMIT,26.5E-12,
MPROP,4,PERMIT,8.85E-12,
C*
C*    VARIABLES FOR POSITIVE, AND NEGATIVE POTENTIALS.
PARASSIGN,POSP,REAL,1,
PARASSIGN,NEGP,REAL,-1,
C*
C*    SET POINT MERGE TOLERANCE
PTTOL,0.000005,
C*
C*    ASSIGN POINTS USING PARAMETRIC VARIABLES TO THE
C*    LEFT BOUNDARY. TPC IN THE X-DIRECTION IS USED SO
C*    THAT THE LEFT BOUNDARY IS NOT ON THE COORDINATE
C*    AXIS (SO THAT THE INFINITE BOUNDARY ELEMENTS WILL
C*    WORK HERE)
PT,1,TPC,0,0,
PT,2,TPC,TPC,0,
PT,3,TPC,TPC+TCOND,0,
C*
C*    FIT DRAWING TO SCREEN
SCALE,0,
C*
C*    CREATE A POINT
```

```
PT,4,TPC,TPC+TFIL,0,
PT,5,TPC,TPC+TFIL+TL1,0,
PT,6,TPC,TPC+TFIL+TL1+TL2,0,
PT,7,TPC,TPC+TFIL+TL1+TL2+TL3,0,
PT,8,TPC,TPC+TFIL+TL1+TL2+TL3+TL4,0,
PT,9,TPC,TPC+TFIL+TL1+TL2+TL3+TL4,TAIR,0,
C*
C*    ASSIGN POINTS TO THE RIGHT BOUNDARY
PT,10,TPC+2*TEDS+19*TLINE+18*TGAP,0,0,
PT,11,TPC+2*TEDS+19*TLINE+18*TGAP,TPC,0,
PT,12,TPC+2*TEDS+19*TLINE+18*TGAP,TPC+TCOND,0,
PT,13,TPC+2*TEDS+19*TLINE+18*TGAP,TPC+TFIL,0,
PT,14,TPC+2*TEDS+19*TLINE+18*TGAP,TPC+TFIL+TL1,0,
PT,15,TPC+2*TEDS+19*TLINE+18*TGAP,TPC+TFIL+TL1+TL2,0,
PT,16,TPC+2*TEDS+19*TLINE+18*TGAP,TPC+TFIL+TL1+TL2+TL3,0,
PT,17,TPC+2*TEDS+19*TLINE+18*TGAP,TPC+TFIL+TL1+TL2+TL3+TL4,0,
PT,18,TPC+2*TEDS+19*TLINE+18*TGAP,TPC+TFIL+TL1+TL2+TL3+TL4+TAIR,0,
C*
C*    FIT DRAWING TO SCREEN
SCALE,0,
C*
C*    ASSIGN THE MAXIMUM NUMBER OF CONDUCTORS, THE 'EQUAL' FLAG, AND
C*    THE COUNTER
PARASSIGN,MAXLIN,INT,19,
PARASSIGN,IEQL,INT,1,
PARASSIGN,ICT,INT,0,
C*
#LOOP L10 MAXLIN
#LOOP L20 2
C*
C*
C*    IF WERE AT THE LEFT SIDE OF A CONDUCTOR...
C*
      #IF (IEQL==1)
PT,,TPC+TEDG+ICT*TLINE+ICT*TGAP,0,0,
PT,,TPC+TEDG+ICT*TLINE+ICT*TGAP,TPC,0,
PT,,TPC+TEDG+ICT*TLINE+ICT*TGAP,TPC+TCOND,0,
PT,,TPC+TEDG+ICT*TLINE+ICT*TGAP,TPC+TFIL,0,
PARRASIGN,IEQL,INT,0,
C*
C*    IF WERE AT THE RIGHT SIDE OF A CONDUCTOR...
C*
      #ELSE
C*
PT,,TPC+TEDG+(1+ICT)*TLINE+ICT*TGAP,0,0,
PT,,TPC+TEDG+(1+ICT)*TLINE+ICT*TGAP,TPC,0,
PT,,TPC+TEDG+(1+ICT)*TLINE+ICT*TGAP,TPC+TCOND,0,
PT,,TPC+TEDG+(1+ICT)*TLINE+ICT*TGAP,TPC+TFIL,0,
PARASSIGN,IEQL,INT,1,
C*
      #ENDIF
C*
#LABEL L20
PARASSIGN,ICT,INT,ICT+1,
#LABEL L10
C*
C*    ACTIVATE THE POINTS,CURVES, AND SURFACES TO PROTECT THEM FROM
C*    BEING ERASED WHEN YOU ERASE HIGHER PRIMITIVES LIKE THE MESHES
C*    YOU CREATE.
ACTKEEP,PT,1,
ACTKEEP,CR,1,
ACTKEEP,SF,1,
C*
C*    VERTICALLY CONNECT THE POINTS ON THE BOUNDARIES
#LOOP L28 8
CRLINE,,CRMAX+1,CRMAX+2,
```

```
#LABEL L28
#LOOP L29 8
CRLINE,,CRMAX+2,CRMAX+3,
#LABEL L29
C*
C*    VERTICALLY CONNECT THE POINTS AT THE COMMON X LOCATION
PARASSIGN,JCNT,INT,2,
#LOOP L30 19*2
#LOOP L40 3
CRLINE,,CRMAX+JCNT+1,CRMAX+JCNT+2,
#LABEL L40
PARASSIGN,JCNT,INT,JCNT+1,
#LABEL L30
C*
C*    CREATE SURFACES ABOVE THE FILLER (CANT START A LOOP WITH A
C*    ZERO LABEL)
SF2CR,1,4,12,0,
SF2CR,2,5,13,0,
SF2CR,3,6,14,0,
SF2CR,4,7,15,0,
SF2CR,5,8,16,0,
C*
C*    NOW THE LEFT END
SF2CR,6,1,17,0,
SF2CR,7,2,18,0,
SF2CR,8,3,19,0,
C*
C*    NOW THE RIGHT END
SF2CR,9,128,9,0,
SF2CR,10,129,10,0,
SF2CR,11,130,11,0,
C*
C*    CREATE SURFACES FROM TWO LINES
C*    FIRST THE AREAS ABOVE, BELOW AND INCLUDING THE GAPS
PARASSIGN,KCNT,INT,9,
#LOOP L50 18
#LOOP L60 3
SF2CR,,SFMAX+KCNT,SFMAX+KCNT+3,0,
#LABEL L60
PARASSIGN,KCNT,INT,KCNT+3,
#LABEL L50
C*
C*    CREATE SURFACES IN THE REGIONS ABOVE AND BELOW THE CONDUCTORS
PARASSIGN,LCNT,INT,0,
#LOOP L70 19
SF2CR,,SFMAX+LCNT-48,SFMAX+LCNT-45,0,
SF2CR,,SFMAX+LCNT-47,SFMAX+LCNT-44,0,
PARASSIGN,LCNT,INT,LCNT+4,
#LABEL L70
C*
C*    ACTIVATE PROPERTIES AND MESH
C*
C*
C*    MESH THE PC BOARD UNDER THE LEFT END...
ACTSET,MP,1,
M_SF,6,6,1,4,16,20,0.08,1,
C*
C*    AND NOW THE RIGHT END
M_SF,9,9,1,4,16,20,0.08,1,
C*
C*    MESH THE PC BOARD UNDER THE GAPS
M_SF,12,63,3,4,16,4,0.08,1,
C*
C*    MESH THE PC BOARD UNDER THE CONDUCTORS
M_SF,66,102,2,4,16,8,0.08,1,
C*
```

```
C*    MESH THE FILLER ON THE LEFT END...
ACTSET,MP,2,
M_SF,7,7,1,4,4,20,1,1,
C*
C*    AND NOW THE RIGHT END
M_SF,10,10,1,4,4,20,1,1,
C*
C*    AND NOW THE GAPS
M_SF,13,64,3,4,4,4,1,1,
C*
C*    MESH THE FILLER ABOVE THE GAPS...
M_SF,14,65,3,4,1,4,1,1,
C*
C*    AND NOW ABOVE THE CONDUCTORS
M_SF,67,103,2,4,1,8,1,1,
C*
C*    MESH THE REGION ABOVE THE LEFT END...
M_SF,8,8,1,4,1,20,1,1,
C*
C*    AND ABOVE THE RIGHT END
M_SF,11,11,1,4,1,20,1,1,
C*
C*    MESH THE FIRST LEVEL ABOVE THE GAGE...
ACTSET,MP,4,
M_SF,1,1,1,4,12,264,1.38,1,
C*
C*    MESH THE SECOND LEVEL ABOVE THE GAGE...
ACTSET,MP,4,
M_SF,2,2,1,4,8,264,1.38,1,
C*
C*    MESH THE THIRD LEVEL...
ACTSET,MP,4,
M_SF,3,3,1,4,6,264,1.38,1,
C*
C*    MESH THE FOURTH LEVEL...
ACTSET,MP,4,
M_SF,4,4,1,4,6,264,2.76,1,
C*
C*    MESH THE AIR...
ACTSET,MP,4,
M_SF,5,5,1,4,4,264,4,1,
C*
C*    SET THE ELEMENT GROUP TO BE 2D ELECTROMAGNETIC PLANAR ELEMENTS
EGROUP,1,MAG2D,0,0,0,0,0,0,0,
C*
C*    SET INFINITE BOUNDARY CONDITION ELEMENTS AT THE LEFT AND RIGHT
C*    BOUNDARIES...
BECR,1,1,1,
BECR,2,2,1,
BECR,3,3,1,
BECR,4,4,1,
BECR,5,5,1,
BECR,6,6,1,
BECR,7,7,1,
BECR,8,8,1,
BECR,9,9,1,
BECR,10,10,1,
BECR,11,11,1,
BECR,12,12,1,
BECR,13,13,1,
BECR,14,14,1,
BECR,15,15,1,
BECR,16,16,1,
C*
C*    AND ALONG THE TOP
BECR,136,136,1,
```

REPORT DOCUMENTATION PAGE

Form Approved
OMB No. 0704-0188

Public reporting burden for this collection of information is estimated to average 1 hour per response, including the time for reviewing instructions, searching existing data sources, gathering and maintaining the data needed, and completing and reviewing the collection of information. Send comments regarding this burden estimate or any other aspect of this collection of information, including suggestions for reducing this burden, to Washington Headquarters Services, Directorate for Information Operations and Reports, 1215 Jefferson Davis Highway, Suite 1204, Arlington, VA 22202-4302, and to the Office of Management and Budget, Paperwork Reduction Project (0704-0188), Washington, DC 20503.

1. AGENCY USE ONLY (Leave blank)	2. REPORT DATE	3. REPORT TYPE AND DATES COVERED
	November 1996	Technical Memorandum

4. TITLE AND SUBTITLE

Design and Laboratory Validation of a Capacitive Sensor for Measuring the Recession of a Thin-Layered Ablator

5. FUNDING NUMBERS

WU 505-68-30

6. AUTHOR(S)

Gregory K. Noffz and Michael P. Bowman

7. PERFORMING ORGANIZATION NAME(S) AND ADDRESS(ES)

NASA Dryden Flight Research Center
P.O. Box 273
Edwards, California 93523-0273

8. PERFORMING ORGANIZATION REPORT NUMBER

H-2111

9. SPONSORING/MONOTORING AGENCY NAME(S) AND ADDRESS(ES)

National Aeronautics and Space Administration
Washington, DC 20546-0001

10. SPONSORING/MONITORING AGENCY REPORT NUMBER

NASA TM-4777

11. SUPPLEMENTARY NOTES

12a. DISTRIBUTION/AVAILABILITY STATEMENT

Unclassified—Unlimited
Subject Category 34

12b. DISTRIBUTION CODE

13. ABSTRACT (Maximum 200 words)

Flight vehicles are typically instrumented with subsurface thermocouples to estimate heat transfer at the surface using inverse analysis procedures. If the vehicle has an ablating heat shield, however, temperature time histories from subsurface thermocouples no longer provide enough information to estimate heat flux at the surface. In this situation, the geometry changes and thermal energy leaves the surface in the form of ablation products. The ablation rate is required to estimate heat transfer to the surface. A new concept for a capacitive sensor has been developed to measure ablator depth using the ablator's dielectric effect on a capacitor's fringe region. Relying on the capacitor's fringe region enables the gage to be flush mounted in the vehicle's permanent structure and not intrude into the ablative heat shield applied over the gage. This sensor's design allows nonintrusive measurement of the thickness of dielectric materials, in particular, the recession rates of low-temperature ablators applied in thin (0.020 to 0.060 in. (0.05 to 0.15 mm)) layers. Twenty capacitive gages with 13 different sensing element geometries were designed, fabricated, and tested. A two-dimensional finite-element analysis was performed on several candidate geometries. Calibration procedures using ablator-simulating shims are described. A one-to-one correspondence between system output and dielectric material thickness was observed out to a thickness of 0.055 in. (1.4 mm) for a material with a permittivity about three times that of air or vacuum. A novel method of monitoring the change in sensor capacitance was developed. This technical memorandum suggests further improvements in gage design and fabrication techniques.

14. SUBJECT TERMS	15. NUMBER OF PAGES
Ablation, Ablation measurement, Capacitive sensors, Fringe field, Thin film measurement	39
	16. PRICE CODE A03

17. SECURITY CLASSIFICATION OF REPORT	18. SECURITY CLASSIFICATION OF THIS PAGE	19. SECURITY CLASSIFICATION OF ABSTRACT	20. LIMITATION OF ABSTRACT
Unclassified	Unclassified	Unclassified	Unlimited

```
C*
C*    SET POTENTIALS AT VERTICAL CONDUCTOR CURVES ON THE MODEL
C*    FIRST POSITIVE...
PARASSIGN,MCNT,INT,0,
#LOOP L85 10
NPCR,18+MCNT*6,POSP,18+MCNT*6+3,3,
PARASSIGN,MCNT,INT,MCNT+2,
#LABEL L85
C*
C*    THEN NEGATIVE
PARASSIGN,NCNT,INT,1,
#LOOP L90 9
NPCR,18+NCNT*6,NEGP,18+NCNT*6+3,3,
PARASSIGN,NCNT,INT,NCNT+2,
#LABEL L90
C*
C*    SET POTENTIALS ALONG THE TOP AND BOTTOM OF CONDUCTORS
NPCR,218,POSP,290,8,
NPCR,219,POSP,291,8,
NPCR,222,NEGP,286,8,
NPCR,223,NEGP,287,8,
C*
C*    SET THE GROUND PLANE
NPCR,137,0,137,1,
NPCR,141,0,141,1,
NPCR,145,0,213,4,
NPCR,217,0,289,4,
C*
C*    MERGE THE NODES AND COMPRESS EXTRANEOUS ONES
NMERGE,1,,1,0.000001,0,1,0,
NCOMPRESS,1,,1,
C*
C*    CALCULATE STORED ELECTRICAL ENERGY
EM_OUTPUT,1,1,0,1,0,0,
C*
C*    ACTIVATE THE EMAGNETIC ANALYSIS MODE USING THE
C*    ELECTROSTATIC OPTION AND GAUSSIAN SOLVER
A_MAGNETIC,E,MKS,0.0001,15,1,0,0,
C*R_CHECK,EMAGNETIC,
R_MAGNETIC
```